

Temporal variations of atmospheric CO₂ and CO at Ahmedabad in western India

Naveen Chandra^{1,2}, Shyam Lal¹, S. Venkataramani¹, Prabir K. Patra³, and Varun Sheel¹

¹Physical Research Laboratory Ahmedabad 380009, India

²Indian Institute of Technology, Gandhinagar 382355, India

³Department of Environmental Geochemical Cycle Research, JAMSTEC, Yokohama, 2360001, Japan

Correspondence to: Shyam Lal (shyam@prl.res.in)

Abstract. About 70% of the anthropogenic carbon dioxide (CO₂) is emitted from the mega-cities and urban areas of the world. In order to draw effective emission mitigation policies for combating future climate change as well as independently validate the emission inventories for constraining their large range of uncertainties, especially over major metropolitan areas of developing countries, there is an urgent need for greenhouse gases measurements over representative urban regions. India is a fast developing country, where fossil fuel emissions have increased dramatically in the last three decades and predicted further to continue to grow by at least 6% per year through 2025. In the absence of systematic CO₂ measurements over the Indian urban locations, CO₂ along with an anthropogenic emission tracer carbon monoxide (CO) are being measured at Ahmedabad, a major urban site in western India, using a state-of-the-art laser based cavity ring down spectroscopy technique from November 2013 to May 2015 with a break during March to June 2014. These measurements enable us to understand the diurnal and seasonal variation in atmospheric CO₂ with respect to its sources (both anthropogenic and biospheric) and biospheric sinks. The observed annual average concentrations of CO₂ and CO are 413.0±13.7 ppm and 0.50±0.37 ppm respectively. Both CO₂ and CO show strong seasonality, with lower concentrations (400.3±6.8 ppm and 0.19±0.13 ppm) during the south-west monsoon and higher concentrations (419.6±22.8 ppm and 0.72±0.68 ppm) during the autumn (SON) season. Strong diurnal variations are also observed for both the species. The common factors for diurnal cycles of CO₂ and CO are the vertical mixing and rush hour traffic, while the influence of biospheric fluxes is also seen in CO₂ diurnal cycle. Using CO and CO₂ covariation, we differentiate the anthropogenic and biospheric components of CO₂ and found that significant contributions of biospheric respiration and anthropogenic emission in the late night (0000 - 0500 hrs) and evening rush hours (1800-2200 hrs) respectively. We compute total yearly emission

of CO to be 69.2 ± 0.07 Gg for the study region using the observed CO:CO₂ correlation slope and bottom-up CO₂ emission inventory. This calculated emission of CO is 52% larger than the estimated emission of CO by the EDGAR inventory. The observations of CO₂ have been compared with an atmospheric chemistry transport model (i.e., ACTM), which incorporates various components of CO₂ fluxes. ACTM is able to capture the basic variabilities, but both diurnal and seasonal amplitudes are largely underestimated compared to the observations. We attribute this underestimation by model to uncertainties in terrestrial biosphere fluxes and coarse model resolution. The fossil fuel signal from the model shows fairly good correlation with observed CO₂ variations, which supports the overall dominance of fossil fuel emissions over the biospheric fluxes in this urban region.

1 Introduction

Carbon dioxide (CO₂) is the most important anthropogenically emitted greenhouse gas (GHG) and has increased substantially from 278 to 390 parts per million (ppm) in the atmosphere since the beginning of the industrial era (circa 1750). It has contributed to more than 65% of the radiative forcing increase since 1750 and hence leads to the significant impact on the climate system (Ciais et al., 2013). Major causes of CO₂ increase are anthropogenic emissions, especially fossil fuel combustion, cement production and land use change. Land and oceans are the two important sinks of atmospheric CO₂, which remove about half of the anthropogenic emissions (Le Quéré et al., 2014). The prediction of future climate change and its feedback rely mostly on our ability to quantifying fluxes of greenhouse gases, especially CO₂ at regional (100-1000 km²) and global scale. Though the global fluxes of CO₂ can be estimated fairly well, the regional scale fluxes are associated with quite high uncertainty especially over the South Asian region; the estimation uncertainty being larger than the value itself (Patra et al., 2013; Peylin et al., 2013). Detailed scientific understanding of the flux distributions is also needed for formulating effective mitigation policies.

Along with the need of atmospheric measurements for predicting the future levels of CO₂, quantifying the components of anthropogenic emissions of CO₂ is similarly important for providing independent verification of mitigation strategies as well as understanding the biospheric component of CO₂. Alone CO₂ measurements could not be helpful in making such study due to the large role of biospheric fluxes in its atmospheric distributions. The proposed strategy for quantification of the anthropogenic component of CO₂ emissions is to measure simultaneously the anthropogenic tracers (Duren and Miller, 2012). CO can be used as a surrogate tracer for detecting and quantifying anthropogenic emissions from burning processes, since it is a major product of incomplete combustion (Turnbull et al., 2006; Wang et al., 2010; Duren and Miller, 2012). The vehicular as well as industrial emissions contribute large fluxes of CO₂ and CO to the atmosphere in urban regions. Several grounds based and aircraft based simultaneous studies of CO and CO₂ have been done in the past

from different parts of the world (Turnbull et al., 2006; Wunch et al., 2009; Wang et al., 2010; Newman et al., 2013) but such study has not been done in India except recently reported results from
60 weekly samples for three Indian sites by Lin et al. (2015).

Measurements at different regions (eg., rural, remote, urban) and at different frequency (eg., weekly, daily, hourly etc) has their own advantage and limitations. For example, the measurements at remote locations at weekly interval can be useful for studying seasonal cycle, growth rate, and
65 estimating the regional carbon sources and sinks after combining their concentrations with inverse modelling and atmospheric tracer transport models. However, some important studies, like their diurnal variations, temporal covariance, etc., are not possible from these measurements due to their limitations. Analysis of temporal covariance of atmospheric mixing processes and variation of flux on shorter time scales, e.g., sub-daily, is essential for understanding local to urban scale CO₂ flux
70 variations (Ahmadov et al., 2007; Pérez-Landa et al., 2007; Briber et al., 2013; Lopez et al., 2013; Ammoura et al., 2014; Ballav et al., 2015). Urban regions contribute about 70% of global CO₂ emission from anthropogenic sources and further projected to increase further over the coming decades (Duren and Miller, 2012). Therefore, measurements over these regions are very helpful for understanding emissions growth as well as verifying the mitigation policies. The first observations of CO₂,
75 CO and other greenhouse gases started in February 1993 from Cape Rama (CRI: a clean site) on the south-west coast of India using flask samples (Bhattacharya et al., 2009). After that, several other groups have initiated the measurements of surface level greenhouse gases (Mahesh et al., 2014; Sharma et al., 2014; Tiwari et al., 2014; Lin et al., 2015). Most of these measurements are made at weakly or fortnightly time intervals or at lower accuracy. Two aircraft based measurement programs, namely, Civil Aircraft for the regular Investigation of the atmosphere Based on an Instrument
80 Container (CARIBIC) (Brenninkmeijer et al., 2007) and Comprehensive Observation Network for TRace gases by AIRliner (CONTRAIL) (Machida et al., 2008) have provided important first look on the South Asian CO₂ budget, but these data have their own limitations (Patra et al., 2011; Schuck et al., 2010, 2012). It is pertinent to mention here that till now, there are no reports of CO₂ measurements over the urban locations of the Indian subcontinent, which could be an important player in the
85 global carbon budget as well as mitigation purpose due to strong growing anthropogenic activities specifically fast growing traffic sector and sinks (large areas of forests and croplands). Hence, the present study is an attempt to reduce this gap by understanding the CO₂ mixing ratios in light of its sources and sinks at an urban region in India.

90

In the view from above, simultaneous continuous measurements of CO₂ and CO have been made since November 2013 from an urban site Ahmedabad located in the western India using very highly sensitive laser based technique. The preliminary results of these measurements for one month period have been reported in (Lal et al., 2015). These detailed measurements are utilized for studying the

95 temporal variations (diurnal and seasonal) of both gases, their emissions characteristics on diurnal
and seasonal scale using their mutual correlations, estimating the contribution of anthropogenic and
biospheric emission components in the diurnal cycle of CO₂ using the ratios of CO to CO₂ and
rough estimate of the annual CO emissions from study region. Finally, the measurements of CO₂
have been compared with simulations using an atmospheric chemistry-transport model to discuss
100 roles of various processes contributing to CO₂ concentrations variations.

2 Site description, local emission sources and meteorology

The measurement facility is housed inside the campus of the Physical Research Laboratory (PRL),
situated in the western part of Ahmedabad (23.03°N, 72.55°E, 55 m AMSL) in the Gujarat state of
105 India (Fig.1). It is a semi-arid, urban region in western India, having a variety of large and small scale
industries (Textile mills and pharmaceutical production facilities) in east and north outskirts. The in-
stitute is situated about 15-20 km away from these industrial areas and surrounded by tree on all
sides. The western part is dominated by the residential areas. The city has a population of about 5.6
million (Census India, 2011) and has large number of automobiles (about 3.2 million), which are in-
110 creasing at the rate of about 10% per year. Most of the city buses and auto-rickshaws (three-wheelers)
use compressed natural gas (CNG) as a fuel. The transport-related activities are the major contribu-
tors of various pollutants (Mallik et al., 2015). An emission inventory for this city, which is devel-
oped for all known sources, shows the annual emissions (for year 2010) of CO₂ and CO about 22.4
million tons and 707,000 tons respectively ([http://www.indiaenvironmentportal.org.in/files/file/Air-](http://www.indiaenvironmentportal.org.in/files/file/Air-Pollution-in-Six-Indian-Cities.pdf)
115 [Pollution-in-Six-Indian-Cities.pdf](http://www.indiaenvironmentportal.org.in/files/file/Air-Pollution-in-Six-Indian-Cities.pdf)). Out of these emissions, transport sector contribute about 36% in
CO₂ emission and 25% in CO emissions, power plants contribute about 32% in CO₂ emissions and
30% in CO emission, industries contribute about 18% in CO₂ emissions and 12% in CO emissions
and domestic sources contribute about 6% in CO₂ emissions and 22% in CO emissions. The Indo-
Gangetic Plain (IGP) is situated in the northeast of Ahmedabad, which is very densely populated
120 region and has high levels of pollutants emitted from various industries and power plants along with
anthropogenic emissions from burning of fossil fuels and traditional biofuels (wood, cow-dung cake
etc). The Thar Desert and the Arabian Sea are situated in the northwest and southwest of Ahmedabad
respectively.

125 Figure 1 shows average monthly variability of temperature, relative humidity (RH), wind speed
based on data taken from Wunderground (<http://www.wunderground.com>), rainfall from Tropical
Rainfall Measuring Mission (TRMM) and planetary boundary layer height (PBLH) from the Modern-
Era Retrospective Analysis for Research and Applications (MEERA). The wind rose plot shows the
surface level wind speed and direction during different seasons over Ahmedabad in 2014. Large sea-

130 sonal variations are observed in the wind speed and direction over Ahmedabad. During the summer monsoon season (June-July-August), the inter-tropical convergence zone (ITCZ) moves northward across India. It results in the transport of moist and cleaner marine air from the Arabian Sea and the Indian Ocean to the study location by south westerly winds, or the so-called southwest monsoon (summer monsoon). The first shower due to the onset of the southwest monsoon occurs in 135 July and it retreats in the mid of September over Ahmedabad. Due to heavy rain and winds mostly from oceanic region, RH shows higher values in July, August and September. Highest RH of about 83% is observed in September. The long-range transport of air masses from the northeast part of the Asian continent starts to prevail over Indian region when ITCZ moves back southward in September and October. These months are regarded as transition period for the monsoon. During autumn 140 (September-October-November), the winds are calm and undergo a change in their direction from south west to north east. When the transition of winds takes place from oceanic to continental region in October, the air gets dryer and RH decreases until December. The winds are north easterly during winter (December- January - February) and transport pollutants mostly from continental region (IGP region). During the spring season (March - April - May), winds are north westerly 145 and little south westerly which transport mixed air masses from continent and oceanic regions. The average wind speed is observed higher in June and July while lower in October and March when transition of wind starts from oceanic to continental and continental to oceanic respectively. The monthly averaged temperature starts increasing from January and attains maximum ($34.6 \pm 1.4^\circ\text{C}$) in June, followed by a decrease until September and temperature is slightly warmer in October compared to the adjacent months. The monthly variation in planetary boundary layer height (PBLH) 150 closely resembles with the temperature pattern. Maximum PBLH of about 1130 m is found in June and it remains in the lower range at about 500 m during July to January. The ventilation coefficient (VC) is obtained by multiplying wind speed and PBL height which gradually increases from January to attain the maximum value in June and the lowest values of VC are observed in October and 155 November.

3 Experiment and model details

3.1 Experimental method

The ambient measurements of CO_2 and CO concentrations have been made using the wavelength scanned cavity ring down spectroscopic (CRDS) technique based analyser (Picarro-G2401) at 0.5 160 Hz. CRDS offers highly sensitive and precise measurements of trace gases in the ambient air, due to its three main characteristics (Bitter et al., 2005; Chen et al., 2010; Karion et al., 2013). (1). It provides very long interaction path length (around 20 km) between the sample and the incident wavelength, by utilizing a 3-mirror configuration, which enhances its sensitivity over other conventional techniques like Non-dispersive Infrared Spectroscopy (NDIR) and Fourier Transform Infrared

165 Spectroscopy (FTIR). (2).The operating low pressure (140 Torr) of cell allows to isolate a single
spectral feature with a resolution of 0.0003 cm^{-1} , which ensures that the peak height or area is lin-
early proportional to the concentration. (3). The measurements of trace gases using this technique are
achieved by measuring the decay time of light intensity inside the cavity while the conventional op-
tical absorption spectroscopy technique is based on absorption of light intensity. Hence, it increases
170 the accuracy of measurements because it is insensitive to the fluctuations of incident light. The cell
temperature of analyzer was maintained at 45°C throughout the study period.

Figure 2 shows the schematic diagram of the experimental set-up, which consists of the analyser,
a glass bulb, a Nafion dryer, a heat less dryer, other associated pumps and a set of calibration mix-
175 tures. Atmospheric air is sampled continuously from the terrace of the building (25 meter above the
ground level) through 1/4 inch PFA Teflon tube via a glass manifold. An external pump is attached
on one side of the glass manifold to flush the sample line. Water vapor affects the measurements of
 CO_2 by diluting its mole fractions in the air and by broadening the spectroscopic absorption lines of
other gases. Although, the instrument has ability to correct for the water vapour interferes by using
180 an experimentally derived water vapor correction algorithms (Crosson, 2008), but it has an absolute
 H_2O uncertainty of $\sim 1\%$ (Chen et al., 2010) and can introduces a source of error using a single
water vapor correction algorithm (Welp et al., 2013). This error can be minimized by either generat-
ing the correction coefficients periodically in the laboratory or by removing the water vapour from
the sample air. Conducting the water vapor correction experiment is bit tricky and need extra care
185 as discussed by Welp et al. (2013). Hence, we prefer to remove water vapour from the sample air
by introducing a 50-strand Nafion dryer (Perma Pure, p/n PD-50T-24MSS) in the upstream of the
analyser. Nafion dryer contains a bunch of semi-permeable membrane tubing separating an internal
sample gas stream from a counter sheath flow of dry gas in stainless steel outer shell. The partial
pressure of water vapour in the sheath air should be lower than the sample air for effectively remov-
190 ing the water vapour from the sample air. A heatless dryer generates dry air using a 4 bar compressor
(KNF, MODEL: NO35ATE) which is used as a sheath flow in Nafion dryer. After drying, sample air
passes through the PTFE filter (polytetrafluoroethylene; $5\mu\text{m}$ Sartorius AG, Germany) before enter-
ing the instrument cavity. This setup dries the ambient air near to 0.03% (300 ppm) concentration of
 H_2O .

195

The measurement system is equipped with three high pressure aluminium cylinders containing
gas mixtures of CO_2 (350.67 ± 0.02 , 399.68 ± 0.01 and 426.20 ± 0.01 ppm) in dry air from NOAA,
Bolder USA, and one cylinder of CO (970 parts per billion (ppb)) from Linde UK. These tanks
were used to calibrate the instrument for CO_2 and CO. An additional gas standard tank (CO_2 : 338
200 ppm, CO: 700 ppb), known as the “target”, is used to monitor the instrumental drift and to assess
the dataset accuracy and repeatability. The target tank values are calibrated against the CO_2 and

CO calibration mixtures. The target tank and calibration gases were measured mostly in the mid of every month (Each calibration gas is passed for 30 minute and target tank for 60 minutes). The target gas is introduced into the instrument for a period of 24 hours also once in a six month, for checking the diurnal variability of instrument drift. Maximum drift for 24 hours has been calculated by subtracting the maximum and minimum value of 5 minute average, which were found to be 0.2 ppm and 0.015 ppm respectively for CO₂ and CO. For all calibration mixtures, the measured concentration is calculated as the average of the last 10 minutes. The linearity of the instrument for CO₂ measurements has been checked by applying the linear fit equation of the CO₂ concentration of the calibration standards (350.67 ppm, 399.68 ppm and 426.20 ppm) measured by the analyzer. The slope is found in the range of 0.99 - 1.007 ppm with a correlation coefficient (r) of about 0.999. Further, linearity of the instrument for CO is also checked by diluting the calibration mixture from 970 ppb to 100 ppb. The calibration mixture is diluted in a glass made dead volume using highly precise and accurate pure air (air free from water vapor, particles, carbon monoxide (CO), sulphur dioxide (SO₂), oxides of nitrogen (NO_x), ozone (O₃), and hydrocarbons (HC)) from ECO Physics generator. The flows of calibration mixture and pure air were regulated using two separate mass flow controllers from Aalborg. For increasing the interaction time of both the gases (zero air and calibration mixture) and to insure a homogeneous mixing, the spring shaped dead volume is used. Each diluted mixture is passed for 30 minutes in the instrument and average of last 10 minute data are used for the test. The instrument shows excellent linearity for CO and slope is observed to be 0.98. The accuracy of the measurements is calculated by subtracting the mean difference of measured CO₂ and CO concentration from the actual concentration of both gases in target gas. The accuracies of CO₂ and CO are found in the range of 0.05-0.2 ppm and 0.01-0.025 ppm respectively. The repeatability of both gases are calculated by the standard deviation of the mean concentration of target gas measured by the analyser over the period of observations and found 0.3 ppm and 0.04 ppm for CO₂ and CO respectively.

3.2 Description of AGCM-based Chemistry Transport Model (ACTM)

This study uses the Center for Climate System Research/National Institute for Environmental Studies/Frontier Research Center for Global Change (CCSR/NIES/FRCGC) atmospheric general circulation model (AGCM)-based chemistry-transport model (ACTM). The model is nudged with reanalysis meteorology using Newtonian relaxation method. The U and V components of horizontal winds are used from the Japan Meteorological Agency Reanalysis (JRA-25) (Onogi et al., 2007). The model has $1.125^{\circ} \times 1.125^{\circ}$ horizontal resolution (T106 spectral truncation) and 32 vertical sigma-pressure layers up to about 50 km. Three components namely anthropogenic emissions, monthly varying ocean exchange with net uptake and terrestrial biospheric exchange of surface CO₂ fluxes are used in the model. The fossil fuel emissions are taken from EDGAR inventory for the year of 2010. Air-sea fluxes from Takahashi et al. (2009) have been used for the oceanic CO₂ tracer.

The oceanic fluxes are monthly and are linearly interpolated between mid-months. The terrestrial biospheric CO₂ tracers are provided from the Carnegie-Ames-Stanford-Approach (CASA) process
240 model (Randerson et al., 1997), after introducing a diurnal variability using 2 m air temperature and surface short wave radiation from the JRA-25 as per Olsen and Randerson (2004). The ACTM simulations has been extensively used in TransCom CO₂ model inter-comparison studies (Law et al., 2008; Patra et al., 2008).

4 Results and Discussion

245 4.1 Time series and general statistics

Figures 3a and 3c show the time series of 30 minute average CO₂ and CO concentrations for the period of November, 2013 - February, 2014 and July, 2014 to May, 2015. Large and periodic variations indicate the stronger diurnal dependence of both the gases. Concentrations and variability of both the gases are observed lowest in the month of July and August, maximum scatter in the concentrations and several plumes of very high levels both gases have been observed from October,
250 2014 until mid-March 2015. Almost all plumes of CO₂ and CO are one to one correlated and are mostly found during evening rush hours and late nights. Figures 3e and 3f show the variations of CO₂ and CO concentrations with wind speed and direction for the study period except July, August and September due to non-availability of wind data. Most of the high and low concentrations of both
255 gases are found to be associated with low and high wind speeds. There is no specific direction for high levels of these gases. This probably indicates the transport sector is an important contributor to the local emissions since the measurement site is surrounded by the city roads.

Figures 3b and 3d show the probability distributions or frequency distributions of CO₂ and CO
260 concentrations during the study period. Both gases show different distributions from each other. This difference could be attributed to the additional role of biospheric cycle (photosynthesis and respiration) on the levels of CO₂ apart from the common controlling factors (local sources, regional transport, PBL dynamics etc) responsible for distributions of both gases. The control of the boundary layer is common for the diurnal variations of these species because of their chemical lifetimes are
265 longer (> months) than the timescale of PBL height variations (~ hrs). However, biospheric fluxes of CO₂ can have strong hourly variations. During the study period the CO₂ concentrations varied between 382 - 609 ppm, with 16% of data lying below 400 ppm, 50% lying in the range 400-420 ppm, 25% between 420-440 ppm and 9% in the range of 440-570 ppm. Maximum frequency of CO₂ is observed at 402.5 ppm during the study period. The CO concentrations lies in the range of
270 0.071-8.8 ppm with almost 8% data lies below the most probable frequency of CO at 0.2 ppm, while 70% data lies between the concentrations of 0.21 ppm and 0.55 ppm. Only 8% data lies above the concentration of 1.6 ppm and rest of 14% data lies between 0.55 and 1.6 ppm. The annual mean

concentrations of CO₂ and CO are found to be 413.0±13.7 ppm and 0.50±0.37 ppm respectively, after removing outliers beyond 2σ values.

275 4.2 Seasonal variations of CO₂ and CO

The seasonal cycles of CO₂ and CO are mostly governed by the strength of emission sources, sinks and transport patterns. Although they follow almost identical seasonal patterns but the factors responsible for their seasonal behaviors are distinct as for the diurnal variations. We calculate the seasonal cycle of CO₂ and CO using two different approaches. In the first approach, we use the monthly
280 mean of all measurements and in the second approach we use monthly mean of the afternoon period (1200-1600 hrs) measurements only. The seasonal cycle from first approach will present the overall variability in both gases. On the other hand, the second approach removes the auto-covariance by excluding CO₂ and CO data mainly affected by local emission sources and represent seasonal cycles at the well mixed volume of the atmosphere. The CO₂ time series is de-trended by subtracting a mean
285 growth rate of CO₂ observed at Mauna Loa (MLO), Hawaii, i.e., 2.13 ppm yr⁻¹ or 0.177 ppm/month (www.esrl.noaa.gov/gmd/ccgg/trends/) for clearly depicting the seasonal cycle amplitude. Figure 4a and Figure 4b show the variations of monthly average concentrations of CO₂ and CO using all daily (0-24 hrs) data and afternoon (1200-1600 hrs) data.

290 In general, total mean values of CO₂ and CO are observed lower in July having concentration 398.78±2.8 ppm and 0.15±0.05 ppm respectively. During summer monsoon months predominance of south-westerly winds which bring cleaner air from the Arabian Sea and the Indian Ocean over to Ahmedabad and high VC (Figure 1) are mostly responsible for the lower concentration of total mean of both the gases. CO₂ and CO concentrations are also at their seasonal low in the northern
295 hemisphere due to net biospheric uptake and seasonally high chemical loss by reaction with OH, respectively. In addition, deep convections in the summer monsoon season efficiently transport the Indian emission (for CO, hydrocarbons) or uptake (for CO₂) signals at the surface to the upper troposphere, resulting lower concentrations at the surface in the summer compared to the winter months (Kar et al., 2004; Randel and Park, 2006; Park et al., 2009; Patra et al., 2011; Baker et al., 2012).
300 During autumn and early winter (December), lower VC values cause trapping of anthropogenically emitted CO₂ and CO and is the major cause for high concentrations of both gases during this period. In addition to this, wind changes from cleaner marine region to polluted continental region, especially from IGP region and hence could be additional factor for higher levels of CO₂ and CO during these seasons (autumn and winter). Elevated levels during these seasons are also examined
305 in several other pollutants over Ahmedabad as discussed in previous studies (Sahu and Lal, 2006; Mallik et al., 2016). Maximum concentrations of CO₂ and CO are observed to be 424.8±17 ppm and 0.83±0.53 ppm, respectively, during November. From January to May the total mean concentration of CO₂ decreases from 415.3±13.6 to 406.1±5.0 ppm and total mean concentration of CO

decreases from 0.71 ± 0.22 to 0.22 ± 0.10 ppm. Higher VC and predominance of comparatively less
310 polluted mixed air masses from oceanic and continental region results in lower total mean concentrations of both gases during this period. There are some clear differences which are observed in the afternoon mean concentrations of CO_2 as compared to daily mean. The first distinct feature is that significant difference of about 5 ppm is observed in the afternoon mean of CO_2 concentration from July to August as compared to the difference in total mean concentration about ~ 0.38 ppm for the
315 same period. Significant differences in the afternoon concentrations of CO_2 from July to August is mainly due to the increasing sink by net biospheric productivity after the Indian summer monsoonal rainfall. Another distinct feature is that the daily mean concentration of CO_2 is found highest in November while the afternoon mean concentration of CO_2 attains maximum value (406 ± 0.4 ppm) in April. Prolonged dry season combined with high daytime temperature (about 41°C) during April-
320 May make the tendency of ecosystem to become moderate source of carbon exchange (Patra et al., 2011) and this could be responsible for the elevated mean noon time concentrations of CO_2 . Unlike CO_2 , seasonal patterns of CO from total and afternoon mean concentrations are identical, although levels are different. It shows that the concentrations of CO is mostly governed by identical sources during day and night time through out the year.

325

The average amplitude (max - min) of the annual cycle of CO_2 is observed around 13.6 and 26.07 ppm from the afternoon mean and total mean respectively. Different annual cycles and amplitudes have been observed from other studies conducted over different Indian stations. Similar to our observations of the afternoon mean concentrations of CO_2 , maximum values are also observed in April at
330 Pondicherry (PON) and Port Blair (PBL) with amplitude of mean seasonal cycles about 7.6 ± 1.4 and 11.1 ± 1.3 ppm respectively (Lin et al., 2015). Cape Rama (CRI), a costal site on the south-west coast of India show the seasonal maxima one month before than our observations in March annual amplitude about 9 ppm (Bhattacharya et al., 2009). The Sinhagad (SNG) site located over the Western Ghats Mountains, show very larger seasonal cycle with annual amplitude about 20 ppm (Tiwari et al.,
335 2014). The amplitude of mean annual cycle at the free tropospheric site Hanle at altitude of 4500 m is observed to be 8.2 ± 0.4 ppm, with maxima in early May and the minima in mid-September (Lin et al., 2015). Distinct seasonal amplitudes and patterns are due to differences in regional controlling factors for the seasonal cycle of CO_2 over these locations, e.g., the Hanle is remotely located from all continental sources, Port Blair site is sampling predominantly marine air, Cape Rama observes
340 marine air in the summer and Indian flux signals in the winter, and Sinhagad represents a forested ecosystem. These comparisons show the need for CO_2 measurements over different ecosystems for constraining its budget.

The annual amplitude in afternoon and daily mean CO concentration is observed to be about 0.27
345 and 0.68 ppm, respectively. The mean annual cycles of CO over PON and PBL show the maxima

in the winter months and minima in summer months same as our observations with annual amplitudes of 0.078 ± 0.01 and 0.144 ± 0.016 ppm, respectively. So the seasonal levels of CO are affected by large scale dynamics which changes air masses from marine to continental and vice versa and by photochemistry. The amplitudes of annual cycle at these locations differ due to their climatic conditions and sources/sinks strengths.

4.3 Diurnal variation

The diurnal patterns for all months and seasons are produced by first generating the time series from the 15 min averages and then averaging the individual hours for all days of the respective month and season after removing the values beyond 2σ - standard deviations for each month as outliers.

4.3.1 Diurnal variation of CO₂

Figure 5a shows the mean diurnal cycles of atmospheric CO₂ and associated $1-\sigma$ standard deviation (shaded region) during all the four seasons. All times are in Indian Standard Time (IST), which is 5.5 hrs ahead of the Universal Time (UT). Noticeable differences are observed in the diurnal cycle of CO₂ from season to season. In general, maximum concentration has been observed during morning (0700-0800 hrs) and evening (1800-2000 hrs) hours, when ABL is shallow, traffic is dense and vegetation respiration dominate due to absence of photosynthetic activity. The minimum of the cycles occurred in the afternoon hours (1400-1600 hrs), when PBL is deepest and well mixed as well as when the vegetation photosynthesis is active. There are many interesting features in the period of 0000-0800 hrs. CO₂ concentrations start decreasing from 0000 to 0300 hrs and increases slightly afterwards till 0600-0700 hrs during summer and autumn. Respiration of CO₂ from the vegetation is mostly responsible for this night time increase. During winter and spring seasons CO₂ levels are observed constant during night hours and small increase is observed only from 0600 to 0800 hrs during the winter season. In contrary to this, subsequent section shows a continuous decline in the night time concentrations of main anthropogenic tracer CO, which indicates that there is enough vertical mixing of low CO air from above that once the CO source is turned off, its concentration drops. Hence, constant levels of CO₂ at night hours during these seasons give the evidence of a continued but weak sources (such as respiration) in order to offset dilution of mixing of low CO₂ air from aloft. Dry soil conditions could be one of the possible causes for weak respirations. Further, distinct timings have been observed in the morning peak of CO₂ during different seasons. It is mostly related to the sunrise time, which will decide the evolutions time of PBL height and beginning of vegetation photosynthesis. The sunrise occurs at 0555-0620 hrs, 0620-0700 hrs, 0700-0723 hrs and 0720-0554 hrs during summer, autumn, winter and spring, respectively. During spring and summer, rush hour starts after sunrise, so the vehicular emissions occur when the PBL has been already high and photosynthetic activity has begun. The CO₂ concentration is observed lowest in the morning during the summer monsoon season as compared to other seasons. This is because CO₂ uptake by

active vegetation deplete entire mixed layer during day time and when the residual layer mixes to the surface in the morning, low-CO₂ air is mixed down. In winter and autumn, rush hour starts parallel with the sunrise, so the emissions occur when the PBL is low and concentration builds up is much stronger in these seasons than in spring and summer seasons.

385

The diurnal amplitude is defined as the difference between the maximum and minimum concentrations of CO₂ in the diurnal cycle. The amplitudes of monthly averaged diurnal cycle of CO₂ from July, 2014 to May 2015 are shown in Figure 5b. The diurnal amplitude shows large month to month variation with increasing trend from July to October and decreasing trend from October onwards.

390 The lowest diurnal amplitude of about 6 ppm is observed in July while highest amplitude about 51 ppm is observed in October. The amplitude does not change largely from December to March and is observed in the range of 25-30 ppm. Similarly from April to May the amplitude also varies in a narrow range from 12 to 15 ppm. The jump in the amplitude of the CO₂ diurnal cycle is observed highest (around 208%) from July to August. This is mainly due to significant increase of biospheric productivity from July to August after the rains in Ahmedabad. It is observed that during July the noon time CO₂ levels are found in the range of 394-397 ppm while in August the noon time levels are observed in the range of 382-393 ppm. The lower levels could be due to the higher PBL height during afternoon and cleaner air, but in case of CO (will be discussed in next section), average day time levels in August are observed higher than in July. It rules out that the lower levels during August are due to the higher PBL height and presence of cleaner marine air, and confirms the higher biospheric productivity during August.

400

Near surface diurnal amplitude of CO₂ has been also documented in humid subtropical Indian station Dehradun and a dry tropical Indian station Gadanki (Sharma et al., 2014). In comparison to Ahmedabad, both these stations show distinct seasonal change in the diurnal amplitude of CO₂. The maximum CO₂ diurnal amplitude of about 69 ppm is observed during the summer season at Dehradun (30.3°N, 78.0°E, 435m), whereas maximum of about 50 ppm during autumn at Gadanki (13.5°N, 79.2°E, 360 m).

405

4.3.2 Diurnal variation of CO

410 Figure 6a shows seasonally averaged diurnal variation of CO. In general, the mean diurnal cycle of CO show lower concentration during noon (1200-1700 hrs) and two peaks in the morning (0800 to 1000 hrs) and in the evening (1800 to 2200 hrs) hours. This cycle exhibits the same pattern as the mean diurnal cycle of traffic flow, with maxima in the morning and at the end of the afternoon, which suggests the influence of traffic emissions on CO measurements. Along with the traffic flow, PBL dynamics also play a critical role in governing the diurnal cycle of CO. The amplitudes of the evening peak in diurnal cycles of CO are always greater than the morning peaks. It is because the

415

PBL height evolves side by side with the morning rush hours traffic and hence increased dilution, while on the other hand, during evening hours, PBL height decrease along with evening dense traffic and favors accumulation of pollutants until the late evening under the stable PBL conditions.

420 The noon time minimum of the cycle is mostly associated with the deepest and well mixed PBL. In general, the average diurnal cycle patterns of both gases (CO_2 and CO) are similar, but having few noticeable differences. The first difference is observed in the timing of the occurrence of morning peaks: CO_2 peaks occur slightly before the CO peak due to the triggering photosynthesis process by the sunrise. On the other hand, the morning peaks of CO mostly depend on the rush hour traffic and

425 are consistent at 0800-1000 hrs in all seasons. The second difference is that the afternoon concentrations of CO show little seasonal spread as compared to the afternoon concentrations of CO_2 . Again, this is due to the biospheric control on the levels of CO_2 during the afternoon hours of different seasons while CO levels are mainly controlled by the dilution during these hours. The third noticeable difference is that the levels of CO decrease very fast after evening rush hours in all the seasons while

430 this feature is not observed in the case of CO_2 since respiration during night hours contributes to the levels of CO_2 . The continuous drop of nighttime concentrations of CO indicates that there is enough vertical mixing of low CO air from above once the CO source is turned off. The average morning (0800-0900 hrs) peak values of CO is observed minimum (0.18 ± 0.1 ppm) in summer and maximum (0.72 ± 0.16 ppm) in winter while evening peak shows minimum value (0.34 ± 0.14 ppm) in summer

435 and maximum (1.6 ± 0.74 ppm) in autumn. The changes in CO concentrations show large fluctuations from morning peak to afternoon minima and from afternoon minima to evening peak. From early morning maxima to noon minima, the changes in CO concentrations are found in the range of 20 -200%, while from noon minima to late evening maxima the changes in CO concentrations are found in the range of 85% to 680%. Similar diurnal variations with two peaks have also been

440 observed in earlier measurements of CO as well as NO_x at this site (Lal et al., 2000).

The evening peak contributes significantly to the diurnal amplitude of CO. The largest amplitude in CO cycle is observed in autumn (1.36 ppm) while the smallest amplitude is observed in summer (0.24 ppm). The diurnal amplitudes of CO are observed to be about 1.01 and 0.62 ppm, respectively

445 during winter and spring. Like CO_2 , the diurnal cycle of CO (Figure 6b) shows the minimum (0.156 ppm) amplitude in July and maximum (1.85 ppm) in October. After October the diurnal amplitude keeps on decreasing till summer. The evening peak contributes significantly to the diurnal amplitude of CO. The largest amplitude in CO cycle is observed in autumn (1.36 ppm) while the smallest amplitude is observed in summer (0.24 ppm). The diurnal amplitudes of CO are observed to be about

450 1.01 and 0.62 ppm, respectively during winter and spring. The monthly diurnal cycle of CO (Figure 6b) shows the minimum (0.156 ppm) amplitude in July and maximum (1.85 ppm) in October. After October the diurnal amplitude keeps on decreasing till monsoon.

4.4 Correlation between CO and CO₂

455 The relationships of CO to CO₂ can be useful for investigating the CO source types and their combustion characteristics in the city region of Ahmedabad. The measurements are generally affected by the dilution due to the boundary layer dynamics, but considering their ratios will cancel this effect. Further, the interpretation of correlation ratios in terms of their dominant emission sources needs to isolate first the local urban signal. For this, the measurements have to be corrected from their
460 background influence. The background concentrations are generally those levels which have almost negligible influence from the local emission sources. Although, the most ideal case of determining the background levels are the continuous measurement of respective gases at a cleaner site. But due to unavailability of such measurements for our study period, we use the 5th percentile value of CO₂ and CO for each day as a background for corresponding day. It is observed that the mixing ratios
465 of both gases at low wind speed, which show the influence of local urban signal, are significantly higher than background levels and hence confirm that the definition of background will not significantly affect the derived ratios (Ammoura et al., 2014). This technique of measuring the background is extensively studied by Ammoura et al. (2014) and found suitable for both the gases CO and CO₂, even having the role of summer uptake on the levels of CO₂. The excess CO₂ (CO_{2(exc)}) and CO
470 (CO_(exc)) above the background for Ahmedabad city, are determined for each day after subtracting the background concentrations from the hours of each day ($CO_{2(exc)} = CO_{2(obs)} - CO_{2(bg)}$, $CO_{(exc)} = CO_{(obs)} - CO_{(bg)}$).

We use robust regression method for the correlation study. It is an alternative to least squares
475 regression method and more applicable for analysing time series data with outliers arising from extreme events (<http://www.ats.ucla.edu/stat/stata/dae/rreg.htm>). Figure 7 illustrates the correlations between CO_(exc) and CO_{2(exc)} for the four seasons at different time windows of the day. Based on the dominance of different atmospheric processes and different emission sources as discussed in Section 4.3, the measurements are divided into the group of four different time windows: (1)
480 Morning period (0600-1000 hrs), when PBL height is slowly evolving and rush hour traffic is there, (2) Afternoon period (1100-1700 hrs), when atmospheric is well mixed and traffic is relatively less, (3) Evening period (1800-2200 hrs), when influence of rush hour traffic is significantly high, (4) Night period (0000-0500 hrs), when atmospheric is calm and the anthropogenic sources of both gases are switched off. The measured slopes values for these time intervals are given in Table 1.
485 The ranges of the emission ratios of CO/CO₂ for transport, industrial and domestic sources, as given in Table 2, are also plotted in the figures for broadly showing the dominance of different sources. The $\Delta CO_{(exc)}/\Delta CO_{2(exc)}$ ratios are observed lowest during summer, with a range varying from 0.9 ppb/ppm in morning to 19.5 ppb/ppm in evening period. Lowest coefficient of determination is also observed during this season, which suggest that the levels of CO and CO₂ are controlled by different
490 factors. As discussed previously, higher biospheric productivity during this season mostly controls

the CO₂ concentrations while CO concentrations are mostly controlled by the long range transport. During the winter season $\Delta\text{CO}_{(exc)}/\Delta\text{CO}_{2(exc)}$ ratios are observed highest and varies from 14.3 ppb/ppm in morning to 47.2 ppb/ppm in evening period. Relatively higher ratios during winter than other three seasons indicates contribution of CO emission from additional biofuel burning sources.

495 From day to night, highest coefficient of determination is observed during spring season. As illustrated by the diurnal cycle, the CO₂ is not significantly removed by the biosphere during spring with lower draw down in daily CO₂. Along with this, higher VC during this season will result in very fast mixing. Therefore, very fast mixing will mostly regulate their relative variation and will result in higher correlation in this season. Other factors like soil and plant respiration during this period

500 may also control CO₂ concentrations due to which the correlation coefficient is not equal to 1. Except monsoon, the $\Delta\text{CO}_{(exc)}/\Delta\text{CO}_{2(exc)}$ ratios and their correlations are fairly comparable in other seasons in the evening rush hours, which indicate stronger influence of common emission sources. Ratios during this time can be considered as fresh emissions since dilution and chemical loss of CO can be considered negligible for this time. Most of these data fall in the domestic and transport sector emission ratio lines, which indicate that during this time intervals these sources mostly

505 dominate (Table 2). On the other hand, during other time intervals most of data is scattered between industrial and transport sectors emission ratio lines. Hence, from this we can conclude that during evening hours, transport and domestic sources mostly dominate while during other periods transport and industrial emission sources mostly dominate. The observed ratios are similar to the air mass influenced by both fossil fuel and biofuel emissions as discussed by Lin et al. (2015) over Pondicherry. Using CARIBIC observations, Lai et al. (2010) also reported the $\Delta\text{CO}/\Delta\text{CO}_2$ ratio in the range of 15.6-29.3 ppb/ppm from the air mass influenced by both biofuel and fossil fuel burning in the Indo-Chinese Peninsula. Further, $\Delta\text{CO}/\Delta\text{CO}_2$ ratio is also observed of about 13 ppb/ppm in South-east Asian outflow in February-April, 2001 during the TRACE-P campaign and suggest the combined

515 influence of fossil fuel and biofuel burning (Russo et al., 2003). The overall ratios (using all data) from autumn to spring (8.4 - 12.7 ppb/ppm) suggest the dominance of local emission sources during these seasons, and this range is correspond to the range of anthropogenic combustion sources (10-15 ppb/ppm) in developed countries (Suntharalingam et al., 2004; Takegawa et al., 2004; Wada et al., 2011). This suggest that the overall emissions of CO over Ahmedabad are mostly dominated by the

520 anthropogenic combustion during these seasons.

If the emissions of CO₂ are known for study locations, the emissions of CO can be estimated by multiplying the correlation slopes and molecular mass mixing ratios (Wunch et al., 2009; Wong et al., 2015). Final emissions of CO will depend on choosing the values of correlation slopes. The

525 slopes should not be biased from particular local sources, chemical processing and PBL dynamics. We exclude the summer monsoon season data as the CO₂ variations mainly depend on the biospheric productivity during this season. As discussed previously, the morning and evening rush hours data

are appropriate for tracking vehicular emissions, while the afternoon data are affected by the other environmental factors, e.g., the PBL dynamics, biospheric activity and chemical process. The stable, shallow night-time PBL accumulates emissions since the evening and hence the correlation slope for this period can be used as a signature of the city's emissions. Hence, we calculate the slopes from the data corresponding to the period of night time (2300-0500 hrs) and evening rush hour (1900-2200 hrs). The CO emission (E_{CO}) for Ahmedabad is calculated using the following formula.

$$E_{CO} = \left(\alpha_{CO} \frac{M_{CO}}{M_{CO_2}} \right) E_{CO_2} \quad (1)$$

Where, α_{CO} is the correlation slope of $CO_{(exc)}$ to $CO_{2(exc)}$ ppb ppm⁻¹, M_{CO} is the molecular mass of CO in g mol⁻¹, M_{CO_2} is the molecular mass of CO₂ in g mol⁻¹ and E_{CO_2} is the CO₂ emission in Gigagram (Gg) over Ahmedabad. The EDGARv4.2 emission inventory reported an annual emissions of CO₂ at 0.1° × 0.1° for the period of 2000-2008 (<http://edgar.jrc.ec.europa.eu/overview.php?v=42>). It reported an annual CO₂ emission of 6231.6 Gg CO₂ yr⁻¹ by EDGARv4.2 inventory over the box (72.3<longitude<72.7°E, 22.8<latitude<23.2°N) which contain Ahmedabad coordinates in center of the box. We assume that the emissions of CO₂ are linearly changing with time and using increasing rate of emission from 2005 to 2008, we extrapolate the emission of CO₂ for 2014 over same area. The bottom-up CO₂ emission for the Ahmedabad is thus estimated of about 8368.6 Gg for the year of 2014. Further, for comparing the estimated emission with inventory emissions we extrapolated the CO emissions also for the year of 2014 using same method applied as for CO₂. Further, we assumed same slopes for the year of 2008 and calculate CO emission for that year also. The slope values for different time period, estimated and inventory emissions of CO using different values of slope are given in Table 3.

The correlation between $CO_{(exc)}$ and $CO_{2(exc)}$ for the period of 2300-0500 hrs is tight and emission are mostly representative of the local anthropogenic sources. Hence, slope for this period can be considered for estimating the fossil fuel CO emissions for Ahmedabad. Further the uncertainty is total emission due to uncertainty associated with used slope is also calculated. Using this slope and based on CO₂ emissions from EDGAR inventory, the estimated fossil fuel emission for CO is observed 69.2±0.7 Gg (emission±uncertainty) for the year of 2014. The EDGAR inventory underestimates the emission of CO as they give the estimate about 45.3 Gg extrapolated for 2014. The slope corresponding to the night hours (1800-0600 hrs) give the highest estimate of CO. Using combinations of slopes for other periods also, the derived CO emissions are larger than the bottom-up EDGAR emission inventory. The EDGAR inventory estimate the relative contributions of CO from industrial, transport and slum/residential sector to be about 42%, 42% and 10%, respectively. The possible cause for underestimation of CO by the EDGAR inventory could be the underestimation of residential emission, since other inventories particularly for major

urban Indian cities (<http://www.indiaenvironmentportal.org.in/files/file/Air-Pollution-in-Six-Indian-Cities.pdf>) show large relative contributions from residential sector. The uncertainty associated with the emission factors for different sectors could be another cause for the underestimation of CO emissions, since these are important parameters for developing the inventory (Sahu et al., 2015).

4.5 Diurnal tracking of CO₂ emissions

CO has virtually no natural source in an urban environments except oxidation of hydrocarbons and hence, can help to disentangle the relative contributions of anthropogenic (from transport, power plant, industrial etc) and the biospheric sources (mainly from respiration) of CO₂, by serving as a tracer of combustion activity attribute CO₂ enhancements to fossil fuel combustion on shorter timescale (Duren and Miller, 2012). Several studies have used the simultaneous time-series measurements of CO₂ and CO to segregate the fraction of CO₂ from anthropogenic sources and natural biospheric sources from its atmospheric concentrations and validated this method using carbon isotope ($\Delta^{14}\text{CO}_2$) measurements (Levin et al., 2003; Turnbull et al., 2006, 2011; Lopez et al., 2013; Newman et al., 2013). This quantification technique is more practical, less expensive and less time consuming in comparison to the $^{14}\text{CO}_2$ method (Vogel et al., 2010). For performing this analysis, the background concentrations of CO and CO₂ and the emission ratio of CO/CO₂ from anthropogenic emissions are required. The methods for calculating the background concentrations of CO₂ and CO are already discussed in Section 4.4. The observed concentrations of both gases can also be directly used for calculating the emission ratio, provided that the measured levels are not highly affected from natural sources as well as share the same origin. We have used the evening time (1900-2100 hrs) data of CO_{2(exc)} and CO_(exc) for whole study period to calculate the emission ratio of CO/CO₂ from predominant anthropogenic emission sources. The emission ratio for this time is calculated to be 47 ± 0.27 ppb CO/ppm CO₂ with very high correlation ($r = 0.95$) (Figure 8b), after excluding those data points, corresponding for which the mean wind speed is greater than 3 ms^{-1} for avoiding the effect of fast ventilation. The tight correlation implies that there is not a substantial difference in the emission ratio of these gases during the measurement period from November, 2013 to May, 2015. CO_{2(exc)} and CO_(exc) will be poorly correlated with each other if their emission ratio varies largely with time, assuming the correlation is mainly driven by emissions. Since anthropogenic emissions are very high for this period, contribution of respiration sources in the levels of CO₂ can be considered negligible during this period. This ratio can be considered as the representative of anthropogenic sources, as discussed in previous section also. We define it as $R_{\text{CO}/\text{CO}_2(\text{ant})}$. The standard deviation shows the uncertainty associated with slope which is very small. The contribution of transport sector (CO_{2(ant)}) in the diurnal cycle of CO₂ is calculated using following formula.

$$CO_{2Veh} = \frac{CO_{obs} - CO_{bg}}{R_{\text{CO}/\text{CO}_2(\text{ant})}} \quad (2)$$

where $CO_{(obs)}$ is the observed CO concentration and $CO_{(bg)}$ is a background CO value. Uncertainty in the $CO_{2(ant)}$ is dominated by the uncertainty in the $R_{CO/CO_{2(ant)}}$ and by the choice of $CO_{(bg)}$. The uncertainty in $CO_{2(ant)}$ due to the uncertainty in the $R_{CO/CO_{2(ant)}}$ is about 0.5% or 600 0.27 ppm and can be considered negligible. As discussed in Section 3, the uncertainty in the measurements of $CO_{(bg)}$ is very small and also can be considered negligible. Further, the contributions of CO_2 from other major sources are calculated by subtracting the $CO_{2(ant)}$ from the excess concentrations of CO_2 . These sources are those sources which do not emit significant amount of CO and can be considered mostly as natural sources (respiration), denoted by $CO_{2(bio)}$.

605

The average diurnal cycles of CO_2 above its background for each season are shown in (Figure 8a). In Section 4.3.1, we have discussed qualitatively the role of different sources in the diurnal cycle of CO_2 . With the help of the above method, now the contributions of anthropogenic ($CO_{2(ant)}$) and biospheric sources ($CO_{2(bio)}$) are discussed quantitatively. Due to unavailability of PBL measurements, we cannot disentangle the contributions of boundary layer dynamics. The diurnal pattern of 610 $CO_{2(ant)}$ (Figure 8c) reflects the pattern like CO, because we are using constant $R_{CO/CO_{2(ant)}}$ for all seasons. Overall, this analysis suggests that the anthropogenic emissions of CO_2 , mostly from transport and industrial sectors during early morning during 0600-1000 hrs varied from 15 to 60% (4-15 ppm). During afternoon hours (1100-1700 hrs), the anthropogenic originated (transport and industrial sources, mainly) CO_2 varied between 20 and 70% (1-11 ppm). During evening rush hours 615 (1800-2200 hrs), highest contributions of combined emissions of anthropogenic sources (mainly transport and domestic) are observed. During this period the contributions vary from 50 to 95% (2-44 ppm). During night/early morning hours (0000-0700 hrs) non-anthropogenic sources (mostly biospheric respiration) contribute from 8 to 41 ppm of CO_2 (Figure 8d). The highest contributions 620 from 18 to 41 ppm are observed in the autumn from the respiration sources during night hours, since there is more biomass during this season after the South Asian summer monsoon. During the afternoon hours, lower biospheric component of CO_2 could be due to a combination of the effects of afternoon anthropogenic emissions, biospheric uptake of CO_2 and higher PBL height.

4.6 Model – Observations comparison

625 4.6.1 Comparison of diurnal cycle of CO_2

We first evaluate the ACTM in simulating the mean diurnal cycle of CO_2 over Ahmedabad by comparing the model simulated surface layer mean diurnal cycle of CO_2 . The atmospheric concentrations of CO_2 are calculated by adding the anthropogenic, oceanic and biospheric component from CASA process model. Figure 9a and Figure 9b show the residuals (Hourly mean - daily mean) of diurnal 630 cycles of CO_2 based on the observations and the model simulations respectively. Model shows very little diurnal amplitude as compared to observations. Larger differences and discrepancies in night

time and morning CO₂ concentrations between the model and observations might be contributed by diurnal cycle of the anthropogenic fluxes from local emissions and biospheric fluxes, and uncertainties in the estimation of PBL height by the model (Law et al., 2008). Hence, there is a need for efforts in improving the regional anthropogenic emissions as well as module for estimating the PBL height. It may be pointed out that the model's horizontal resolution ($1.125^{\circ} \times 1.125^{\circ}$) is coarse for analysing local scale observations. However, the model is able to capture the trend of the diurnal amplitude, highest in autumn and lowest in the summer monsoon season. Figure 9c shows better agreement ($r = 0.75$) between the monthly change in modelled and observational diurnal amplitude of CO₂ from monthly mean diurnal cycle however slope ($m = 0.17$) is very poor. We include the diurnal amplitudes of CO₂ for November and December, 2013 also for improving the total number of data points. The model captured the spread in the day time concentration of CO₂ from summer to spring with a difference that the model shows lower concentration of CO₂ during noon hours in autumn while observations show lowest in the summer monsoon season.

645

The monthly average diurnal cycles of the biospheric net primary productivity from the CASA model for Ahmedabad and for the year of 2014 are shown Figure 10. The details of CASA flux are given in the Section 3.2. It is clear from Figure 10 that the CO₂ flux diurnal cycle as modelled by CASA show minimum day-night variations amplitude during the summer monsoon time (Jun-July-August). Given that biosphere over Ahmedabad is water stressed for all other three seasons (except the summer monsoon time, Figure 1A3), the behaviour of CASA model simulated diurnal variation is not in line with biological capacity of the plants to assimilate atmospheric CO₂. Due to this underestimation of CO₂ uptake in the summer monsoon season, we also find very large underestimation of the seasonal through by ACTM in comparison with observations (Figure 9). Hence, there is a discrepancy in the diurnal flux of CO₂ simulated by CASA model. Similar discrepancy in the timing of maximum biospheric uptake is also discussed earlier by Patra et al. (2011) using inverse model CO₂ fluxes and CASA biospheric fluxes. It clearly suggest that there is a need for improving the biospheric flux for this region. It should be mentioned here that the CASA model used a land use map corresponding the late 1980s and early 1990s, which should be replaced by rapid growth in urbanised area in Ahmedabad (area and population increased by 91% and 42%, respectively, between 1990 and 2011). The model resolutions may be another factor for discrepancy. As Ballav et al. (2012) show that a regional model WRF-CO₂ is able to capture both diurnal and synoptic variations at two closely spaced stations within 25 km. Hence the regional models could be helpful for capturing these variabilities.

665

4.6.2 Comparison of seasonal cycle of CO₂

Figure 11a shows the performance of ACTM simulating mean seasonal cycle of CO₂ over Ahmedabad by comparing the model simulated mean surface seasonal cycle of CO₂. Due to unavailability of data from March, 2014 to June, 2014 we plotted the monthly average of the year 2015 for same periods for visualizing the complete seasonal cycle of CO₂. The seasonal cycles are calculated after subtracting the annual mean from each month, and corrected for growth rate using the observations at MLO. For comparison, we used the seasonal cycle calculated from afternoon time average monthly concentrations, since the model is not able to capture the local fluctuations and produce better agreements when boundary layer is well mixed. In Table 4 we present the summary of the comparisons of the model and observations. The model reproduces the observed seasonal cycle in CO₂ fairly well but with low seasonal amplitude about 4.15 ppm compared to 13.6 ppm observed. Positive bias during the summer monsoon season depicts the underestimation of biospheric productivity by the CASA model. The root mean square error is observed highest to be 3.21% in the summer monsoon season. For understanding the role of biosphere, we also compared the seasonal cycle of CO₂ from noon time mean data with the seasonal cycle of CO₂ fluxes over South Asia region which is taken from the Patra et al. (2011) where they calculated it using a inverse model with including CARIBIC data and shifted a sink of 1.5Pg C yr⁻¹ sink from July to August and termed it as “TDI64/CARIBIC-modified”. Positive and negative values of flux show the net release and net sink by the land biosphere over the South Asia. This comparison shows almost one to one correlation in the monthly variation of CO₂ and suggest that the lower levels of CO₂ during July, August and higher level in April are mostly due to the moderate source and sink of South Asian ecosystem during these months respectively. Significant correlation ($r = 0.88$) between South Asian CO₂ fluxes and monthly mean CO₂ data for day time only suggest that the day time levels of CO₂ are mostly controlled by the seasonal cycle of biosphere (Figure 11b).

690

Separate correlations of each CO₂ tracer with the observations are helpful to determine relative importance of each flux component in the CO₂ variation (Patra et al., 2008). Hence, we perform separate correlation study between the measurements and biospheric, anthropogenic and oceanic component of CO₂, estimated by model using CASA-3hr fluxes (Randerson et al., 1997; Olsen and Randerson, 2004), EDGAR v4.2 inventory and air-sea fluxes from Takahashi et al. (2009) respectively. The correlation coefficient give the hint about dominating controlling factors of deriving the levels of CO₂. Figure 11b shows the resulting correlations for separate flux component with respect to measurements. We did not include the oceanic tracer and observed CO₂ correlation result, since no correlation has been observed between them. The comparison is based on daily mean of entire time series. Correlation between biospheric tracers and observed CO₂ have been found negative. This is because during growing season biospheric sources act as a net sink for CO₂. Correlation of observed CO₂ with fossil fuel tracer has been observed fairly well ($r = 0.75$). Hence, individual

700

tracers correlation study also give the evidence of the overall dominance of fossil flux in overall concentrations of CO₂ over Ahmedabad for entire study period, and by assuming fossil fuel CO₂ emission we can derive meaningful information on biospheric uptake cycle.

This study suggest that the model is able to capture seasonal cycle with lower amplitude for Ahmedabad. However, the model fails to capture the diurnal variability since local transport and hourly daily flux play important roles for governing the diurnal cycle and hence there is a need for improving these features of the model.

5 Conclusions

Atmospheric concentrations of CO₂ were measured along with an anthropogenic tracer CO at Ahmedabad, a semiarid urban region in western India using laser based CRDS technique during 2013-2015. The air masses, originated from both polluted continental regions as well as cleaner marine regions over the study location during different seasons, make this study most important for studying the characteristics of both type of air masses (polluted and relatively cleaner). The observations show large range of variability in CO₂ concentrations (from 382 to 609 ppm) and CO concentrations (from 0.07 to 8.8 ppm), with the average of 416 ± 19 ppm and 0.61 ± 0.6 ppm respectively. The higher concentrations of both the gases are recorded for lower ventilation and for winds from north-east direction, while lowest concentrations are observed for higher ventilation and for the cleaner south-west winds from the Indian Oceanic region. Along with these factors, the biospheric activity also controls the seasonal cycle of CO₂. Lowest day time CO₂ concentrations ranging from 382–393 ppm in August, suggest for the stronger biospheric productivity during this month over the study region, in agreement with an earlier inverse modelling study. This is in contrast to the terrestrial flux simulated by the CASA ecosystem model, showing highest productivity in September and October months. Hence, the seasonal cycles of both the gases reflect the seasonal variations of natural sources/sinks, anthropogenic emissions and seasonally varying atmospheric transport. The annual amplitudes of CO₂ variation after subtracting the growth rate based on the Mauna Loa, Hawaii data are observed to be about 26.07 ppm using monthly mean of all the data and 13.6 ppm using monthly mean of the afternoon period (1200-1600 hrs) data only. Significant difference between these amplitudes suggests that the annual amplitude from afternoon monthly mean data only does not give true picture of the variability. It is to be noted that most of the CO₂ measurements in India are based on day time flask samplings only.

Significant differences in the diurnal patterns of CO₂ and CO are also observe, even though both the gases have major common emission sources and undergo PBL dynamics and advection. Differences in their diurnal variability is probably the effect of terrestrial biosphere on CO₂ and chemical

loss of CO due to reaction with OH radicals. The morning and evening peaks of CO are affected by rush hours traffic and PBL height variability and occur almost same time throughout the year. 740 However, the morning peaks in CO₂ changes its time slightly due to shift in photosynthesis activity according to change in sun rise time during different seasons. The amplitudes of annual average diurnal cycles of CO₂ and CO are observed about 25 and 0.48 ppm respectively (Table 5). Both gases show highest amplitude in the autumn and lowest in the summer monsoon season. This shows that major influencing processes are common for both the gases, specific to this city and the monsoon 745 India.

The availability of simultaneous and continuous measurements of CO₂ and CO have made it possible to study their correlations at different time windows (during morning (0600-1000 hrs), noon (1100-1700 hrs), evening (1800-2200) and night (0000-0500 hrs) hours) of distinct seasons. Using 750 the correlation slopes and comparing them with the emission ratios of different sources, contributions of distinct sources is discussed qualitatively. It is observed that during the evening hours, measurements over the study region are mostly affected by transport and domestic sources, while during other periods the levels of both gases are mostly dominated by the emissions from transport and industrial sources. Further, using the slope from the evening rush hours (1800-2200 hrs) data as 755 anthropogenic emission ratios, the relative contributions of dominant anthropogenic emissions and biospheric emissions have been disentangle from the diurnal cycle of CO₂. At rush hours, this analysis suggests that 90-95% of the total emissions of CO₂ are contributed by anthropogenic emissions. The total yearly emission of CO for Ahmedabad has been also estimated using these measurements. In this estimation, fossil fuel derived emission of CO₂ from EDGAR v4.2 inventory is extrapolated 760 linearly from 2008 to 2014 and it is assumed that there are no year-to-year variations in the land biotic and oceanic CO₂ emissions. The estimated annual emission CO for Ahmedabad is estimated to be 69.2±0.7 Gg for the year of 2014. The extrapolated CO emission from EDGAR inventory for 2014 shows a value smaller than this estimate by about 52%.

765 The observed results of CO₂ are also compared with an atmospheric general circulation model based chemistry transport model simulated CO₂ concentrations. The model captures some basic features like the trend of diurnal amplitude, seasonal amplitude etc, qualitatively but not quantitatively. The model captures the seasonal cycle fairly good but the amplitude is very less as compared to the observations. Similarly, performance of the model capturing the change in monthly averaged diurnal 770 amplitude is quiet good ($r = 0.72$), however the slope is very poor. We also examined the correlation between the hourly averaged observed CO₂ and tracer of fossil fuel from model simulation and found fairly good correlation between them. However, no significant correlation has been observed between observed CO₂ and biospheric tracer. It suggests that the levels of CO₂ over Ahmedabad are

mostly controlled by the fossil fuel combustion throughout the year.

775

This work demonstrate the usefulness of simultaneous measurements of CO₂ and CO in an urban region. The anthropogenic and biospheric component of CO₂ have been studied from its temporally varying atmospheric concentrations, and validity of “bottom-up” inventory have been assessed independently. Use of CO_(exc):CO_{2(exc)} ratios avoid some of the problems with assumptions that have to be made with modelling. These results represent a major urban region of India and will be helpful in validating emission inventories, chemistry-transport and terrestrial ecosystem models. However, a bigger network of sites is needed to elucidate more accurate distribution of emissions and their source regions, and run continuously over multiple years for tracking the changes associated with anthropogenic activities and emission mitigation policies.

780

785 *Acknowledgements.* The authors greatly acknowledge the PRL and ISROGBP-ATCTM for funding and support. We acknowledge the support of Mr. T.K. Sunil Kumar in making the measurements. We thank the European Commission for the provision of the EDGAR inventory data used in this study. We thank the reviewers for their exhaustive comments and detailed suggestions in getting the MS to its present form. We are grateful to the editor for his support throughout the review process.

790 The corresponding author may be contacted for the data published in this article.

References

- Ahmadov, R., Gerbig, C., Kretschmer, R., Koerner, S., Neininger, B., Dolman, A. J., and Sarrat, C.: Mesoscale covariance of transport and CO₂ fluxes: Evidence from observations and simulations using the WRF-VPRM coupled atmosphere-biosphere model, *Journal of Geophysical Research: Atmospheres*, 112, doi:10.1029/2007JD008552, d22107, 2007.
- 795 Ammoura, L., Xueref-Remy, I., Gros, V., Baudic, A., Bonsang, B., Petit, J.-E., Perrussel, O., Bonnaire, N., Sciare, J., and Chevallier, F.: Atmospheric measurements of ratios between CO₂ and co-emitted species from traffic: a tunnel study in the Paris megacity, *Atmospheric Chemistry and Physics*, 14, 12 871–12 882, doi:10.5194/acp-14-12871-2014, 2014.
- 800 Andreae, M. O. and Merlet, P.: Emission of trace gases and aerosols from biomass burning, *Global Biogeochemical Cycles*, 15, 955–966, doi:10.1029/2000GB001382, 2001.
- Baker, A. K., Schuck, T. J., Brenninkmeijer, C. A. M., Rauthe-Schöch, A., Slemr, F., van Velthoven, P. F. J., and Lelieveld, J.: Estimating the contribution of monsoon-related biogenic production to methane emissions from South Asia using CARIBIC observations, *Geophysical Research Letters*, 39, doi:10.1029/2012GL051756,
- 805 110813, 2012.
- Ballav, S., PATRA, P. K., TAKIGAWA, M., GHOSH, S., DE, U. K., MAKSYUTOV, S., MURAYAMA, S., MUKAI, H., and HASHIMOTO, S.: Simulation of CO₂ Concentration over East Asia Using the Regional Transport Model WRF-CO₂, *Journal of the Meteorological Society of Japan. Ser. I*, 90, 959–976, doi:10.2151/jmsj.2012-607, 2012.
- 810 Ballav, S., Patra, P. K., Sawa, Y., Matsueda, H., Adachi, A., Onogi, S., Takigawa, M., and De, U.: Simulation of CO₂ concentrations at Tsukuba tall tower using WRF–CO₂ tracer transport model, *J. Earth System Sci.*, in press, 2015.
- Bhattacharya, S. K., Borole, D. V., Francey, R. J., Allison, C. E., Steele, L. P., Krummel, P., Langenfelds, R., Masarie, K. A., Tiwari, Y. K., and Patra, P.: Trace gases and CO₂ isotope records from Cabo de Rama, India,
- 815 *Current Science*, 97, 2009.
- Bitter, M., Ball, S. M., Povey, I. M., and Jones, R. L.: A broadband cavity ringdown spectrometer for in-situ measurements of atmospheric trace gases, *Atmospheric Chemistry and Physics*, 5, 2547–2560, doi:10.5194/acp-5-2547-2005, 2005.
- Brenninkmeijer, C. A. M., Crutzen, P., Boumard, F., Dauer, T., Dix, B., Ebinghaus, R., Filippi, D., Fischer, H., Franke, H., Frieß, U., Heintzenberg, J., Helleis, F., Hermann, M., Kock, H. H., Koepfel, C., Lelieveld, J., Leuenberger, M., Martinsson, B. G., Miemczyk, S., Moret, H. P., Nguyen, H. N., Nyfeler, P., Oram, D., O’Sullivan, D., Penkett, S., Platt, U., Pupek, M., Ramonet, M., Randa, B., Reichelt, M., Rhee, T. S., Rohwer, J., Rosenfeld, K., Scharffe, D., Schlager, H., Schumann, U., Slemr, F., Sprung, D., Stock, P., Thaler, R., Valentino, F., van Velthoven, P., Waibel, A., Wandel, A., Waschitschek, K., Wiedensohler, A., Xueref-Remy,
- 825 I., Zahn, A., Zech, U., and Ziereis, H.: Civil Aircraft for the regular investigation of the atmosphere based on an instrumented container: The new CARIBIC system, *Atmospheric Chemistry and Physics*, 7, 4953–4976, doi:10.5194/acp-7-4953-2007, 2007.
- Briber, B. M., Hutyra, L. R., Dunn, A. L., Raciti, S. M., and Munger, J. W.: Variations in Atmospheric CO₂ Mixing Ratios across a Boston, MA Urban to Rural Gradient, *Land*, 2, 304, doi:10.3390/land2030304, 2013.

- 830 CAO, G., ZHANG, X., GONG, S., and ZHENG, F.: Investigation on emission factors of particulate matter and gaseous pollutants from crop residue burning, *Journal of Environmental Sciences*, 20, 50 – 55, doi:[http://dx.doi.org/10.1016/S1001-0742\(08\)60007-8](http://dx.doi.org/10.1016/S1001-0742(08)60007-8), 2008.
- Chen, H., Winderlich, J., Gerbig, C., Hofer, A., Rella, C. W., Crosson, E. R., Van Pelt, A. D., Steinbach, J., Kolle, O., Beck, V., Daube, B. C., Gottlieb, E. W., Chow, V. Y., Santoni, G. W., and Wofsy, S. C.: High-accuracy continuous airborne measurements of greenhouse gases (CO₂ and CH₄) using the cavity ring-down spectroscopy (CRDS) technique, *Atmospheric Measurement Techniques*, 3, 375–386, doi:10.5194/amt-3-375-2010, 2010.
- 835 Ciais, P., Sabine, C., Bala, G., Bopp, L., Brovkin, V., Canadell, J., Chhabra, A., DeFries, R., Galloway, J., Heimann, M., Jones, C., Quere, C., Myneni, R., Piao, S., and Thornton, P.: Carbon and Other Biogeochemical Cycles, book section 6, p. 465–570, Cambridge University Press, Cambridge, United Kingdom and New York, NY, USA, doi:10.1017/CBO9781107415324.015, 2013.
- 840 Crosson, E.: A cavity ring-down analyzer for measuring atmospheric levels of methane, carbon dioxide, and water vapor, *Applied Physics B*, 92, 403–408, doi:10.1007/s00340-008-3135-y, 2008.
- Dhammapala, R., Claiborn, C., Simpson, C., and Jimenez, J.: Emission factors from wheat and Kentucky blue-grass stubble burning: Comparison of field and simulated burn experiments, *Atmospheric Environment*, 41, 1512 – 1520, doi:<http://dx.doi.org/10.1016/j.atmosenv.2006.10.008>, 2007.
- 845 Duren, R. M. and Miller, C. E.: Measuring the carbon emissions of megacities, *Nature Clim. Change*, 2, 560–562, doi:<http://dx.doi.org/10.1038/nclimate1629>, 2012.
- Kar, J., Bremer, H., Drummond, J. R., Rochon, Y. J., Jones, D. B. A., Nichitiu, F., Zou, J., Liu, J., Gille, J. C., Edwards, D. P., Deeter, M. N., Francis, G., Ziskin, D., and Warner, J.: Evidence of vertical transport of carbon monoxide from Measurements of Pollution in the Troposphere (MOPITT), *Geophysical Research Letters*, 31, doi:10.1029/2004GL021128, 2004.
- 850 Karion, A., Sweeney, C., Wolter, S., Newberger, T., Chen, H., Andrews, A., Kofler, J., Neff, D., and Tans, P.: Long-term greenhouse gas measurements from aircraft, *Atmospheric Measurement Techniques*, 6, 511–526, doi:10.5194/amt-6-511-2013, 2013.
- 855 Lai, S. C., Baker, A. K., Schuck, T. J., van Velthoven, P., Oram, D. E., Zahn, A., Hermann, M., Weigelt, A., Slemr, F., Brenninkmeijer, C. A. M., and Ziereis, H.: Pollution events observed during CARIBIC flights in the upper troposphere between South China and the Philippines, *Atmospheric Chemistry and Physics*, 10, 1649–1660, doi:10.5194/acp-10-1649-2010, 2010.
- 860 Lal, S., Naja, M., and Subbaraya, B.: Seasonal variations in surface ozone and its precursors over an urban site in India, *Atmospheric Environment*, 34, 2713 – 2724, doi:[http://dx.doi.org/10.1016/S1352-2310\(99\)00510-5](http://dx.doi.org/10.1016/S1352-2310(99)00510-5), 2000.
- Lal, S., Chandra, N., and Venkataramani, S.: A study of CO₂ and related trace gases using a laser based technique at an urban site in western India., *Current Science*, 109, 2015.
- 865 Law, R. M., Peters, W., Rödenbeck, C., Aulagnier, C., Baker, I., Bergmann, D. J., Bousquet, P., Brandt, J., Bruhwiler, L., Cameron-Smith, P. J., Christensen, J. H., Delage, F., Denning, A. S., Fan, S., Geels, C., Houweling, S., Imasu, R., Karstens, U., Kawa, S. R., Kleist, J., Krol, M. C., Lin, S.-J., Lokupitiya, R., Maki, T., Maksyutov, S., Niwa, Y., Onishi, R., Parazoo, N., Patra, P. K., Pieterse, G., Rivier, L., Satoh, M., Serrar, S., Taguchi, S., Takigawa, M., Vautard, R., Vermeulen, A. T., and Zhu, Z.: TransCom model simulations of hourly atmo-

- 870 spheric CO₂: Experimental overview and diurnal cycle results for 2002, *Global Biogeochemical Cycles*, 22, doi:10.1029/2007GB003050, gB3009, 2008.
- Le Quéré, C., Moriarty, R., Andrew, R. M., Peters, G. P., Ciais, P., Friedlingstein, P., Jones, S. D., Sitch, S., Tans, P., Arneeth, A., Boden, T. A., Bopp, L., Bozec, Y., Canadell, J. G., Chevallier, F., Cosca, C. E., Harris, I., Hoppema, M., Houghton, R. A., House, J. I., Jain, A., Johannessen, T., Kato, E., Keeling, R. F., Kitidis, 875 V., Klein Goldewijk, K., Koven, C., Landa, C. S., Landschützer, P., Lenton, A., Lima, I. D., Marland, G., Mathis, J. T., Metzl, N., Nojiri, Y., Olsen, A., Ono, T., Peters, W., Pfeil, B., Poulter, B., Raupach, M. R., Regnier, P., Rödenbeck, C., Saito, S., Salisbury, J. E., Schuster, U., Schwinger, J., Séférian, R., Segschneider, J., Steinhoff, T., Stocker, B. D., Sutton, A. J., Takahashi, T., Tilbrook, B., van der Werf, G. R., Viovy, N., Wang, Y.-P., Wanninkhof, R., Wiltshire, A., and Zeng, N.: Global carbon budget 2014, *Earth System Science* 880 *Data Discussions*, 7, 521–610, doi:10.5194/essdd-7-521-2014, 2014.
- Levin, I., Kromer, B., Schmidt, M., and Sartorius, H.: A novel approach for independent budgeting of fossil fuel CO₂ over Europe by ¹⁴CO₂ observations, *Geophysical Research Letters*, 30, doi:10.1029/2003GL018477, 2194, 2003.
- Lin, X., Indira, N. K., Ramonet, M., Delmotte, M., Ciais, P., Bhatt, B. C., Reddy, M. V., Angchuk, D., Balakrishnan, S., Jorphail, S., Dorjai, T., Mahey, T. T., Patnaik, S., Begum, M., Brenninkmeijer, C., Durairaj, S., Kirubakaran, R., Schmidt, M., Swathi, P. S., Vinithkumar, N. V., Yver Kwok, C., and Gaur, V. K.: Long-lived 885 atmospheric trace gases measurements in flask samples from three stations in India, *Atmospheric Chemistry and Physics*, 15, 9819–9849, doi:10.5194/acp-15-9819-2015, 2015.
- Lopez, M., Schmidt, M., Delmotte, M., Colomb, A., Gros, V., Janssen, C., Lehman, S. J., Mondelain, D., 890 Perrussel, O., Ramonet, M., Xueref-Remy, I., and Bousquet, P.: CO, NO_x and ¹³CO₂ as tracers for fossil fuel CO₂: results from a pilot study in Paris during winter 2010, *Atmospheric Chemistry and Physics*, 13, 7343–7358, doi:10.5194/acp-13-7343-2013, 2013.
- Machida, T., Matsueda, H., Sawa, Y., Nakagawa, Y., Hirofumi, K., Kondo, N., Goto, K., Nakazawa, T., Ishikawa, K., and Ogawa, T.: Worldwide Measurements of Atmospheric CO₂ and Other Trace Gas Species Using 895 Commercial Airlines, *J. Atmos. Oceanic Technol.*, 25, 1744–1754, doi:10.1175/2008JTECHA1082.1, 2008.
- Mahesh, P., Sharma, N., Dadhwal, V., Rao, P., Apparao, B., Ghosh, A., Mallikarjun, K., and Ali, M.: Impact of Land-Sea Breeze and Rainfall on CO₂ Variations at a Coastal Station, *Journal of Earth Science and Climatic Change*, 5, –, doi:10.4172/2157-7617.1000201, 2014.
- Mallik, C., Lal, S., and Venkataramani, S.: Trace gases at a semi-arid urban site in western India: variability and 900 inter-correlations, *Journal of Atmospheric Chemistry*, pp. 1–22, doi:10.1007/s10874-015-9311-7, 2015.
- Mallik, C., Chandra, N., Venkataramani, S., and Lal, S.: Variability of atmospheric carbonyl sulfide at a semi-arid urban site in western India, *Science of The Total Environment*, 551–552, 725 – 737, doi:http://dx.doi.org/10.1016/j.scitotenv.2016.02.014, 2016.
- Newman, S., Jeong, S., Fischer, M. L., Xu, X., Haman, C. L., Lefter, B., Alvarez, S., Rappenglueck, B., Kort, 905 E. A., Andrews, A. E., Peischl, J., Gurney, K. R., Miller, C. E., and Yung, Y. L.: Diurnal tracking of anthropogenic CO₂ emissions in the Los Angeles basin megacity during spring 2010, *Atmospheric Chemistry and Physics*, 13, 4359–4372, doi:10.5194/acp-13-4359-2013, http://www.atmos-chem-phys.net/13/4359/2013/, 2013.

- Olsen, S. C. and Randerson, J. T.: Differences between surface and column atmospheric CO₂ and implications
910 for carbon cycle research, *Journal of Geophysical Research: Atmospheres*, 109, doi:10.1029/2003JD003968,
<http://dx.doi.org/10.1029/2003JD003968>, d02301, 2004.
- Onogi, K., Tsutsui, J., Koide, H., Sakamoto, M., Kobayashi, S., Hatsushika, H., Matsumoto, T., Yamazaki,
N., Kamahori, H., Takahashi, K., Kadokura, S., Wada, K., Kato, K., Oyama, R., Ose, T., Mannoji, N., and
915 Taira, R.: The JRA-25 Reanalysis, *Journal of the Meteorological Society of Japan. Ser. II*, 85, 369–432,
doi:10.2151/jmsj.85.369, 2007.
- Park, M., Randel, W. J., Emmons, L. K., and Livesey, N. J.: Transport pathways of carbon monoxide in the Asian
summer monsoon diagnosed from Model of Ozone and Related Tracers (MOZART), *Journal of Geophysical
Research: Atmospheres*, 114, doi:10.1029/2008JD010621, 2009.
- Patra, P. K., Law, R. M., Peters, W., Rödenbeck, C., Takigawa, M., Aulagnier, C., Baker, I., Bergmann, D. J.,
920 Bousquet, P., Brandt, J., Bruhwiler, L., Cameron-Smith, P. J., Christensen, J. H., Delage, F., Denning, A. S.,
Fan, S., Geels, C., Houweling, S., Imasu, R., Karstens, U., Kawa, S. R., Kleist, J., Krol, M. C., Lin, S.-J.,
Lokupitiya, R., Maki, T., Maksyutov, S., Niwa, Y., Onishi, R., Parazoo, N., Pieterse, G., Rivier, L., Satoh, M.,
Serrar, S., Taguchi, S., Vautard, R., Vermeulen, A. T., and Zhu, Z.: TransCom model simulations of hourly
atmospheric CO₂: Analysis of synoptic-scale variations for the period 2002–2003, *Global Biogeochemical
925 Cycles*, 22, doi:10.1029/2007GB003081, gB4013, 2008.
- Patra, P. K., Niwa, Y., Schuck, T. J., Brenninkmeijer, C. A. M., Machida, T., Matsueda, H., and Sawa, Y.: Carbon
balance of South Asia constrained by passenger aircraft CO₂ measurements, *Atmospheric Chemistry and
Physics*, 11, 4163–4175, doi:10.5194/acp-11-4163-2011, 2011.
- Patra, P. K., Canadell, J. G., Houghton, R. A., Piao, S. L., Oh, N.-H., Ciais, P., Manjunath, K. R., Chhabra, A.,
930 Wang, T., Bhattacharya, T., Bousquet, P., Hartman, J., Ito, A., Mayorga, E., Niwa, Y., Raymond, P. A., Sarma,
V. V. S. S., and Lasco, R.: The carbon budget of South Asia, *Biogeosciences*, 10, 513–527, doi:10.5194/bg-
10-513-2013, 2013.
- Pérez-Landa, G., Ciais, P., Gangoiti, G., Palau, J. L., Carrara, A., Gioli, B., Miglietta, F., Schumacher, M.,
Millán, M. M., and Sanz, M. J.: Mesoscale circulations over complex terrain in the Valencia coastal region,
935 Spain - Part 2 : Modeling CO₂ transport using idealized surface fluxes, *Atmospheric Chemistry and Physics*,
7, 1851–1868, doi:10.5194/acp-7-1851-2007, 2007.
- Peylin, P., Law, R. M., Gurney, K. R., Chevallier, F., Jacobson, A. R., Maki, T., Niwa, Y., Patra, P. K., Peters, W.,
Rayner, P. J., Rödenbeck, C., van der Laan-Luijkx, I. T., and Zhang, X.: Global atmospheric carbon budget:
results from an ensemble of atmospheric CO₂ inversions, *Biogeosciences*, 10, 6699–6720, doi:10.5194/bg-
940 10-6699-2013, 2013.
- Randel, W. J. and Park, M.: Deep convective influence on the Asian summer monsoon anticyclone and asso-
ciated tracer variability observed with Atmospheric Infrared Sounder (AIRS), *Journal of Geophysical Re-
search: Atmospheres*, 111, doi:10.1029/2005JD006490, 2006.
- Randerson, J. T., Thompson, M. V., Conway, T. J., Fung, I. Y., and Field, C. B.: The contribution of terrestrial
945 sources and sinks to trends in the seasonal cycle of atmospheric carbon dioxide, *Global Biogeochemical
Cycles*, 11, 535–560, doi:10.1029/97GB02268, 1997.
- Russo, R. S., Talbot, R. W., Dibb, J. E., Scheuer, E., Seid, G., Jordan, C. E., Fuelberg, H. E., Sachse, G. W.,
Avery, M. A., Vay, S. A., Blake, D. R., Blake, N. J., Atlas, E., Fried, A., Sandholm, S. T., Tan, D., Singh,

- H. B., Snow, J., and Heikes, B. G.: Chemical composition of Asian continental outflow over the western Pacific: Results from Transport and Chemical Evolution over the Pacific (TRACE-P), *Journal of Geophysical Research: Atmospheres*, 108, doi:10.1029/2002JD003184, 2003.
- 950 Sahu, L. and Lal, S.: Distributions of C₂–C₅ {NMHCs} and related trace gases at a tropical urban site in India, *Atmospheric Environment*, 40, 880 – 891, doi:http://dx.doi.org/10.1016/j.atmosenv.2005.10.021, 2006.
- Sahu, S., Beig, G., and Parkhi, N.: High Resolution Emission Inventory of NO_x and CO for Mega City Delhi, India, *Aerosol and Air Quality Research*, 15, 1137–1144, doi:10.4209/aaqr.2014.07.0132, 2015.
- 955 Schuck, T. J., Brenninkmeijer, C. A. M., Baker, A. K., Slemr, F., von Velthoven, P. F. J., and Zahn, A.: Greenhouse gas relationships in the Indian summer monsoon plume measured by the CARIBIC passenger aircraft, *Atmospheric Chemistry and Physics*, 10, 3965–3984, doi:10.5194/acp-10-3965-2010, 2010.
- Schuck, T. J., Ishijima, K., Patra, P. K., Baker, A. K., Machida, T., Matsueda, H., Sawa, Y., Umezawa, T., Brenninkmeijer, C. A. M., and Lelieveld, J.: Distribution of methane in the tropical upper troposphere measured by CARIBIC and CONTRAIL aircraft, *Journal of Geophysical Research: Atmospheres*, 117, doi:10.1029/2012JD018199, d19304, 2012.
- 960 Sharma, N., Dadhwal, V., Kant, Y., Mahesh, P., Mallikarjun, K., Gadavi, H., Sharma, A., and Ali, M.: Atmospheric CO₂ Variations in Two Contrasting Environmental Sites Over India, *Air, Soil and Water Research*, 7, 61–68, doi:10.4137/ASWR.S13987, 2014.
- 965 Streets, D. G., Bond, T. C., Carmichael, G. R., Fernandes, S. D., Fu, Q., He, D., Klimont, Z., Nelson, S. M., Tsai, N. Y., Wang, M. Q., Woo, J.-H., and Yarber, K. F.: An inventory of gaseous and primary aerosol emissions in Asia in the year 2000, *Journal of Geophysical Research: Atmospheres*, 108, doi:10.1029/2002JD003093, 2003.
- 970 Suntharalingam, P., Jacob, D. J., Palmer, P. I., Logan, J. A., Yantosca, R. M., Xiao, Y., Evans, M. J., Streets, D. G., Vay, S. L., and Sachse, G. W.: Improved quantification of Chinese carbon fluxes using CO₂/CO correlations in Asian outflow, *Journal of Geophysical Research: Atmospheres*, 109, doi:10.1029/2003JD004362, 2004.
- Sánchez-Ccoylo, O., Ynoue, R., Martins, L., Astolfo, R., Miranda, R., Freitas, E., Borges, A., Fornaro, A., Freitas, H., Moreira, A., and Andrade, M.: Vehicular particulate matter emissions in road tunnels in Sao Paulo, Brazil, *Environmental Monitoring and Assessment*, 149, 241–249, doi:10.1007/s10661-008-0198-5, 2009.
- 975 Takahashi, T., Sutherland, S. C., Wanninkhof, R., Sweeney, C., Feely, R. A., Chipman, D. W., Hales, B., Friederich, G., Chavez, F., Sabine, C., Watson, A., Bakker, D. C., Schuster, U., Metzl, N., Yoshikawa-Inoue, H., Ishii, M., Midorikawa, T., Nojiri, Y., Körtzinger, A., Steinhoff, T., Hoppema, M., Olafsson, J., Arnarson, T. S., Tilbrook, B., Johannessen, T., Olsen, A., Bellerby, R., Wong, C., Delille, B., Bates, N., and de Baar, H. J.: Climatological mean and decadal change in surface ocean pCO₂, and net sea–air {CO₂} flux over the global oceans, *Deep Sea Research Part II: Topical Studies in Oceanography*, 56, 554 – 577, doi:http://dx.doi.org/10.1016/j.dsr2.2008.12.009, 2009.
- 985 Takegawa, N., Kondo, Y., Koike, M., Chen, G., Machida, T., Watai, T., Blake, D. R., Streets, D. G., Woo, J.-H., Carmichael, G. R., Kita, K., Miyazaki, Y., Shirai, T., Liley, J. B., and Ogawa, T.: Removal of NO_x and NO_y in Asian outflow plumes: Aircraft measurements over the western Pacific in January 2002, *Journal of Geophysical Research: Atmospheres*, 109, doi:10.1029/2004JD004866, 2004.

- 990 Tiwari, Y. K., Vellore, R. K., Kumar, K. R., van der Schoot, M., and Cho, C.-H.: Influence of monsoons on atmospheric CO₂ spatial variability and ground-based monitoring over India, *Science of The Total Environment*, 490, 570 – 578, doi:<http://dx.doi.org/10.1016/j.scitotenv.2014.05.045>, 2014.
- Turnbull, J. C., Miller, J. B., Lehman, S. J., Tans, P. P., Sparks, R. J., and Southon, J.: Comparison of ¹⁴CO₂, CO, and SF₆ as tracers for recently added fossil fuel CO₂ in the atmosphere and implications for biological CO₂ exchange, *Geophysical Research Letters*, 33, doi:10.1029/2005GL024213, 2006.
- 995 Turnbull, J. C., Karion, A., Fischer, M. L., Faloona, I., Guilderson, T., Lehman, S. J., Miller, B. R., Miller, J. B., Montzka, S., Sherwood, T., Saripalli, S., Sweeney, C., and Tans, P. P.: Assessment of fossil fuel carbon dioxide and other anthropogenic trace gas emissions from airborne measurements over Sacramento, California in spring 2009, *Atmospheric Chemistry and Physics*, 11, 705–721, doi:10.5194/acp-11-705-2011, 2011.
- Vogel, F. R., HAMMER, S., STEINHOF, A., KROMER, B., and LEVIN, I.: Implication of weekly and diurnal ¹⁴C calibration on hourly estimates of CO-based fossil fuel CO₂ at a moderately polluted site in southwestern Germany, *Tellus B*, 62, 512–520, doi:10.1111/j.1600-0889.2010.00477.x, 2010.
- 1000 Wada, A., Matsueda, H., Sawa, Y., Tsuboi, K., and Okubo, S.: Seasonal variation of enhancement ratios of trace gases observed over 10 years in the western North Pacific, *Atmospheric Environment*, 45, 2129 – 2137, doi:<http://dx.doi.org/10.1016/j.atmosenv.2011.01.043>, 2011.
- 1005 Wang, Y., Munger, J. W., Xu, S., McElroy, M. B., Hao, J., Nielsen, C. P., and Ma, H.: CO₂ and its correlation with CO at a rural site near Beijing: implications for combustion efficiency in China, *Atmospheric Chemistry and Physics*, 10, 8881–8897, doi:10.5194/acp-10-8881-2010, 2010.
- Welp, L. R., Keeling, R. F., Weiss, R. F., Paplawsky, W., and Heckman, S.: Design and performance of a Nafion dryer for continuous operation at CO₂ and CH₄ air monitoring sites, *Atmospheric Measurement Techniques*, 6, 1217–1226, doi:10.5194/amt-6-1217-2013, 2013.
- 1010 Westerdahl, D., Wang, X., Pan, X., and Zhang, K. M.: Characterization of on-road vehicle emission factors and microenvironmental air quality in Beijing, China, *Atmospheric Environment*, 43, 697 – 705, doi:<http://dx.doi.org/10.1016/j.atmosenv.2008.09.042>, 2009.
- Wong, K. W., Fu, D., Pongetti, T. J., Newman, S., Kort, E. A., Duren, R., Hsu, Y.-K., Miller, C. E., Yung, Y. L., and Sander, S. P.: Mapping CH₄: CO₂ ratios in Los Angeles with CLARS-FTS from Mount Wilson, California, *Atmospheric Chemistry and Physics*, 15, 241–252, doi:10.5194/acp-15-241-2015, 2015.
- 1015 Wunch, D., Wennberg, P. O., Toon, G. C., Keppel-Aleks, G., and Yavin, Y. G.: Emissions of greenhouse gases from a North American megacity, *Geophysical Research Letters*, 36, doi:10.1029/2009GL039825, 2009.

Table 1: Correlation slopes ($\Delta\text{CO}_{(exc)}/\Delta\text{CO}_2_{(exc)}$ in ppb/ppm) measured during different time intervals of distinct seasons. Coefficient of determination (r^2) is given inside the bracket.

Seasons	Slope in ppb/ppm (Coefficient of determination (r^2))			
	Morning (0600-1000 hrs)	Afternoon (1100-1700 hrs)	Evening (1800-2200 hrs)	Night (0000-0500 hrs)
Summer (JA)	0.9 (0.15)	10.0 (0.17)	19.5 (0.67)	0.5 (0.16)
Autumn (SON)	8.3 (0.48)	14.1 (0.75)	45.2 (0.90)	35.3 (0.71)
Winter (DJF)	14.3 (0.51)	20.0 (0.68)	47.2 (0.90)	30.0 (0.75)
Spring (MAM)	9.3 (0.68)	18.0 (0.80)	43.7 (0.93)	26.0 (0.80)

Table 2: Emission ratios of CO/CO₂ (ppb/ppm), derived from emission factors (gram of gases emitted per kilogram of fuel burned).

Biomass burning	Transport		Industry	Domestic	
Crop-residue ^{a,b,c}	Diesel ^{d,e,f}	Gasoline ^{d,f}	Coal	Coal ^{d,f}	Biofuel ^{c,d}
45.7-123.6	8.6-65.2	33.5	23.5-40.4	53.3-62.2	52.9-98.5

^aDhammapala et al. (2007); ^bCAO et al. (2008); ^cAndreae and Merlet (2001); ^dStreets et al. (2003); ^eSánchez-Ccoyllo et al. (2009); ^fWesterdahl et al. (2009)

Table 3: Estimates of emissions of CO using the the CO₂ emission from EDGAR inventory over the box (72.3<longitude<72.7°E, 22.8<latitude<23.2°N) and observed CO_(exc):CO₂(exc) slopes for different time periods. The correlation coefficient for corresponding slopes are given inside the bracket in slope column. Data for the summer monsoon season are not included for calculating slopes.

Time (IST)	Slope (ppb/ppm)	EDGAR Emissions (Gg/yr)		Estimated Emissions Gg(yr)
	Correlation coefficient (r)	CO ₂	CO	
2300 - 0500 hrs	13±0.14 (0.84)	8368.6	45.3	69.2±0.7
1900 - 2100 hrs	47±0.27 (0.95)			250.2±1.5

Table 4: Performance matrices used to quantify the level of agreement between the model simulations and observations. These statistics are based on hourly values in each day.

Parameter	Winter	Autumn	Summer	All months
MB (ppm)	-2.72	12.64	-2.45	2.27
FGE (%)	0.96	3.12	2.0	1.76
RMSE (ppm)	5.21	12.82	9.14	8.60
RMSE (%)	1.27	3.21	2.20	2.09

Table 5: Seasonal mean concentrations and diurnal amplitudes (max-min) of CO₂ and CO over Ahmedabad.

Period	Mean (ppm)		Diurnal amplitude (ppm)	
	CO ₂	CO	CO ₂	CO
Monsoon	400.3±6.8	0.19±0.13	12.4	0.24
Autumn	419.6±22.8	0.72±0.71	40.9	1.36
Winter	417.2±18.5	0.73±0.68	31.7	1.01
Spring	415.4±14.8	0.41±0.40	15.9	0.62
Annual	413.0±13.7	0.50±0.37	25.0	0.48

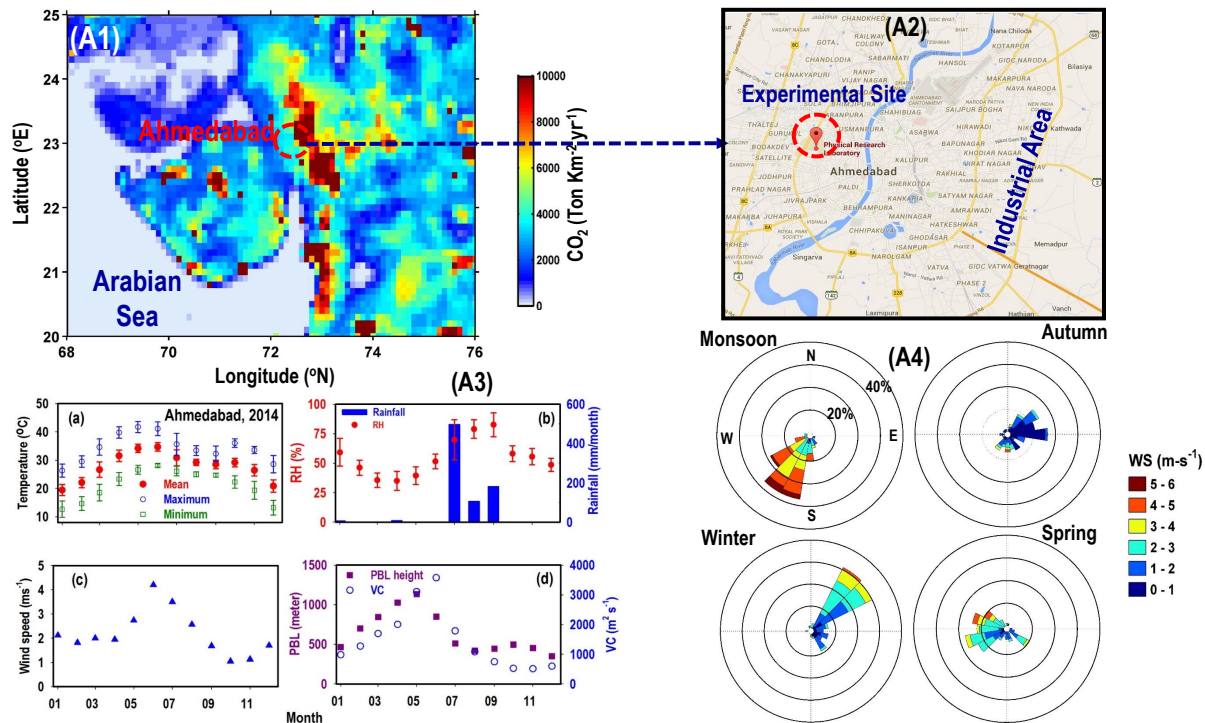


Figure 1: (A1) Spatial distribution of total anthropogenic CO₂ emissions from the EDGARv4.2 inventory over Ahmedabad and surrounding regions. (A2) The Ahmedabad city map showing location of the experimental site (PRL). (A3: a-d) Monthly average temperature with monthly maximum and minimum value, relative humidity (RH), rainfall, wind speed, PBL height and ventilation coefficient (VC) over Ahmedabad during the year 2014. Temperature, RH and wind speed are taken from Wunderground weather (www.wunderground.com) while rainfall and PBLH data are used from Tropical Rainfall Measuring Mission (TRMM) satellite and MEERA reanalysis data. (A4) Wind rose plots for Ahmedabad for the four seasons of 2014 using daily average data from Wunderground.

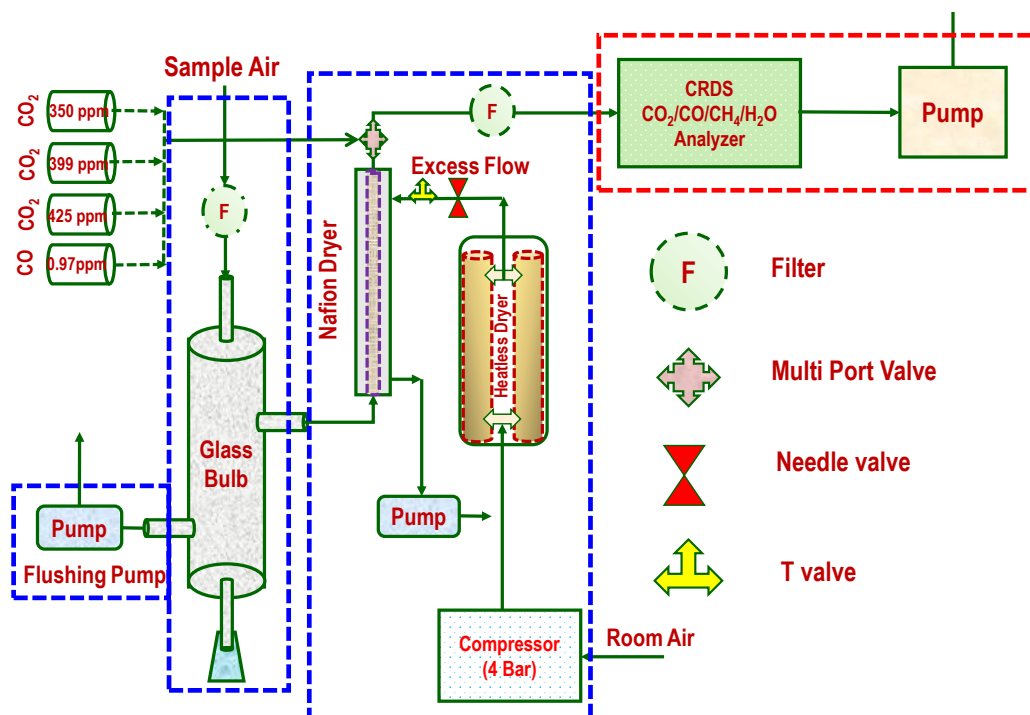


Figure 2: Schematic diagram of the experimental set-up. We introduce additionally a Nafion dryer upstream of the inlet of instrument for removing the water vapour. Three calibration mixtures from NOAA, USA are used to calibrate CO₂ measurements and one calibration mixture from Linde, UK is used to calibrate CO measurements. The red color box covers the analyser system received from the company, while two blue colours box cover the two stage moisture removing systems, designed at our lab in PRL.

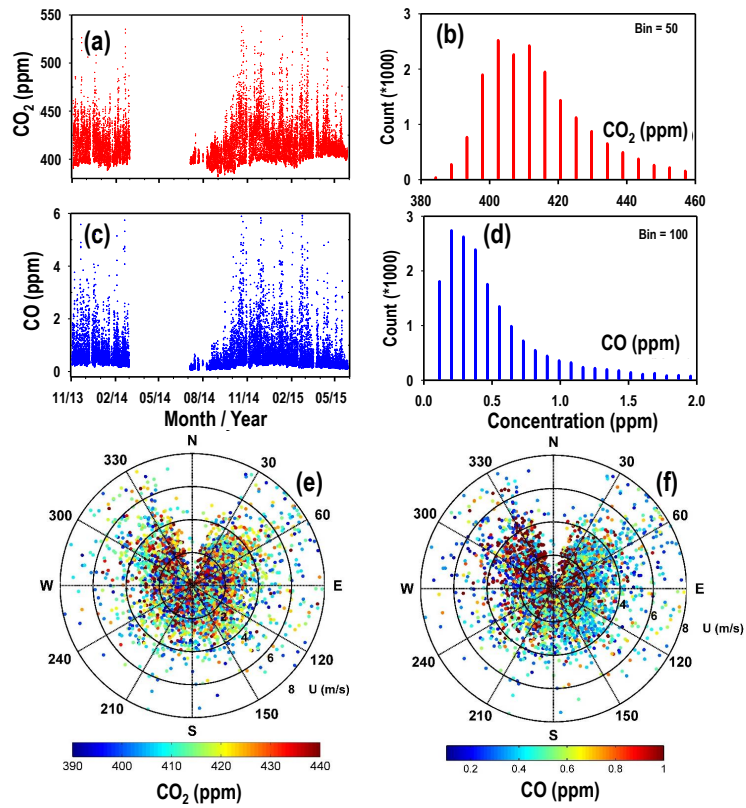


Figure 3: (a and c) Time series of 30 minute average values CO₂ and CO measured at Ahmedabad for the study period. (b and d) The frequency distribution in CO₂ and CO concentrations for the study period using 30 minute mean of both gases. (e and f) The polar plots show the variation of 30 minute averaged CO₂ and CO at this site with wind direction and speed during the study period except July, August and September due to unavailability of meteorology data.

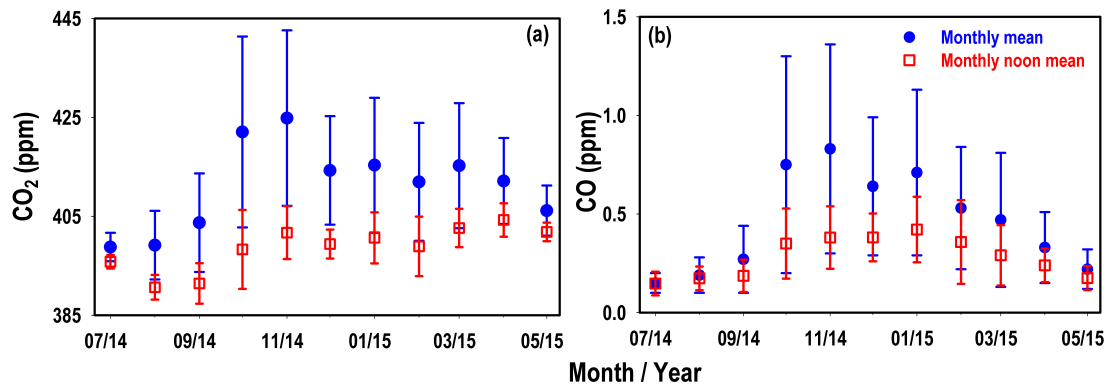


Figure 4: The seasonal variation of CO₂ and CO from July, 2014 to May, 2015 using their monthly mean concentrations. The blue dots and red rectangles show the monthly average concentrations of these gases for the total (0-24 hrs) and noon time (1200-1600 hrs) data respectively with 1σ spread.

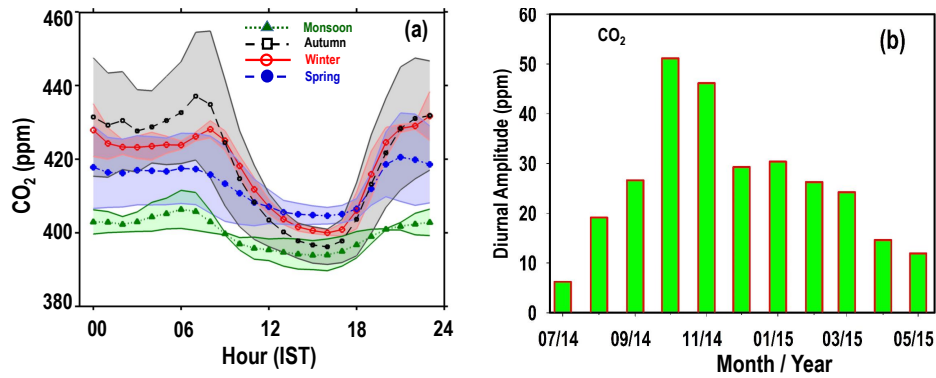


Figure 5: (a) Average diurnal variation of CO₂ over Ahmedabad during all the four seasons. (b) Monthly variation of average diurnal amplitude of CO₂ during from July, 2014 to May, 2015. All times are in Indian Standard Time (IST), which is 5.5 hrs ahead of Universal Time (UT).

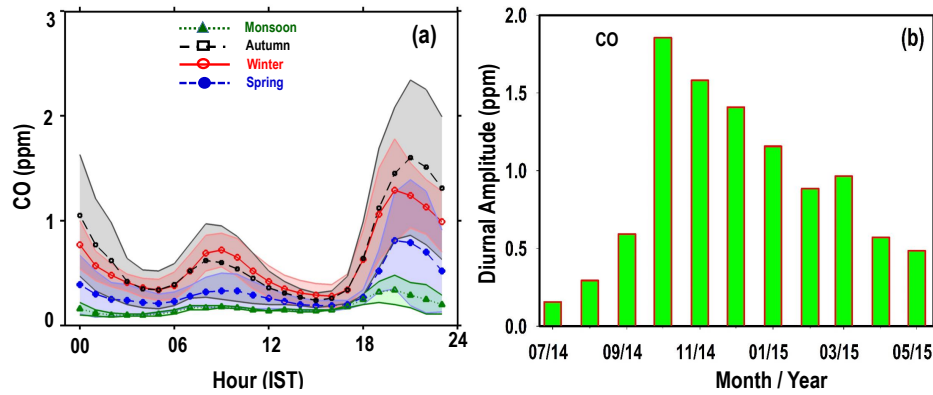


Figure 6: (a) Diurnal variation of CO over Ahmedabad during all the four seasons. (b) Monthly variation of the diurnal amplitude of CO.

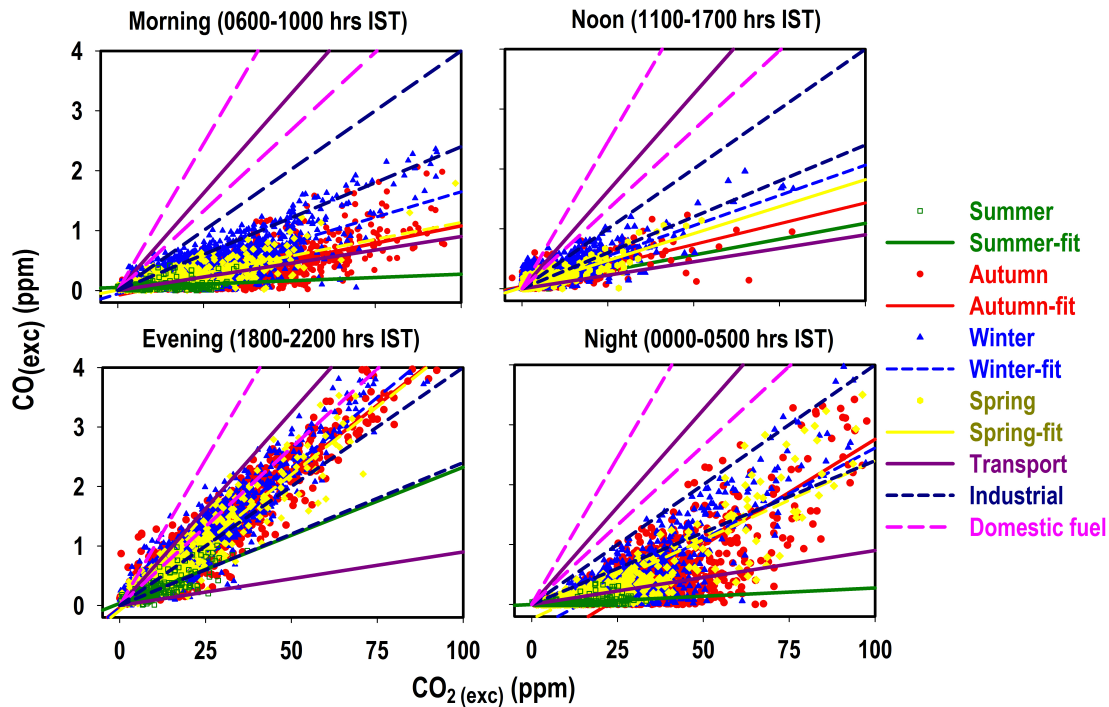


Figure 7: Scatter plots and regression fits of excess CO (CO_{exc}) vs. excess CO_2 ($CO_{2(exc)}$) during morning (0600-1000 hrs), noon (1100-1700 hrs), evening (1800-2200) and night (0000-0500 hrs) hours for all the four different seasons. Excess values of both species are calculated after subtracting their background concentrations. Each data points are averaged for 30 minutes. Emission ratios range of CO/CO_2 for different sources from the literature are also plotted in each figure.

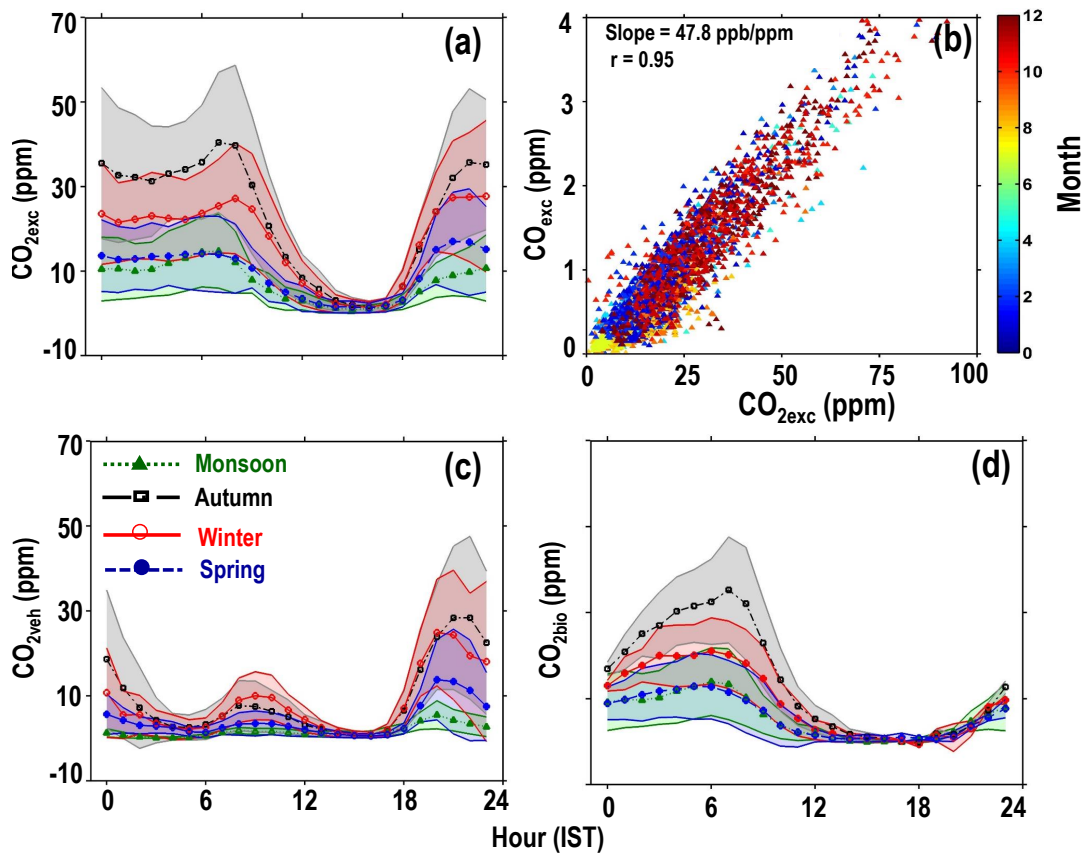


Figure 8: (a) Diurnal cycle of excess CO₂ over background levels during all the four seasons. (b) Correlation between excess CO and CO₂ for evening hours (1800-2100 hrs) during the study period. Contributions of fossil fuel (c) and biosphere (d) in the diurnal variation of excess CO₂ in all the four seasons.

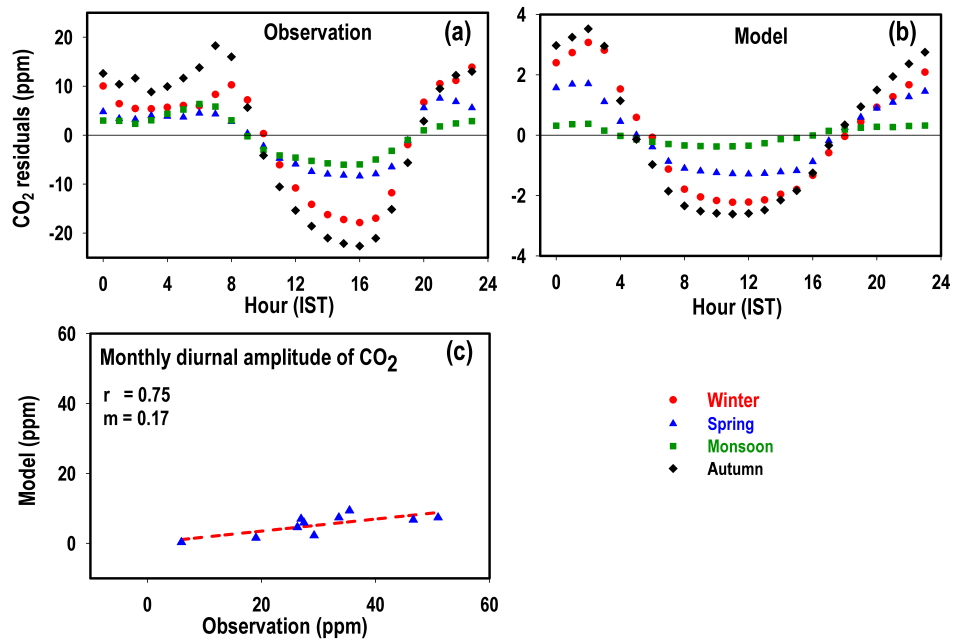


Figure 9: Residual of the diurnal cycle of CO₂ (in ppm) for (a) observations and (b) model simulation over Ahmedabad in all the four seasons. Please note that the scales of the model and observational diurnal cycles are different. (c) Correlation between observed and the model simulated monthly mean diurnal cycle amplitudes.

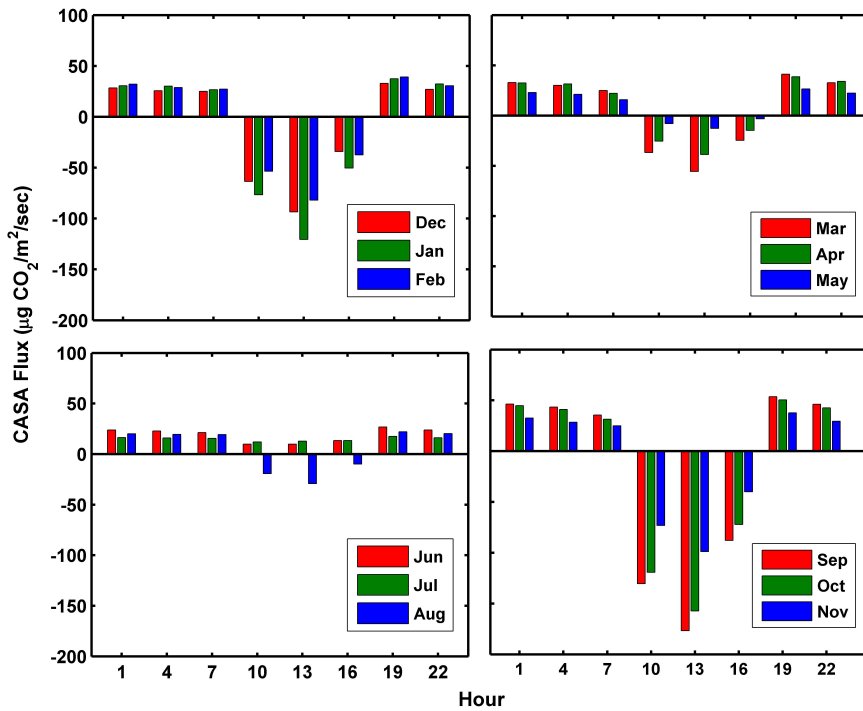


Figure 10: Diurnal variation of biospheric fluxes from the CASA ecosystem model.

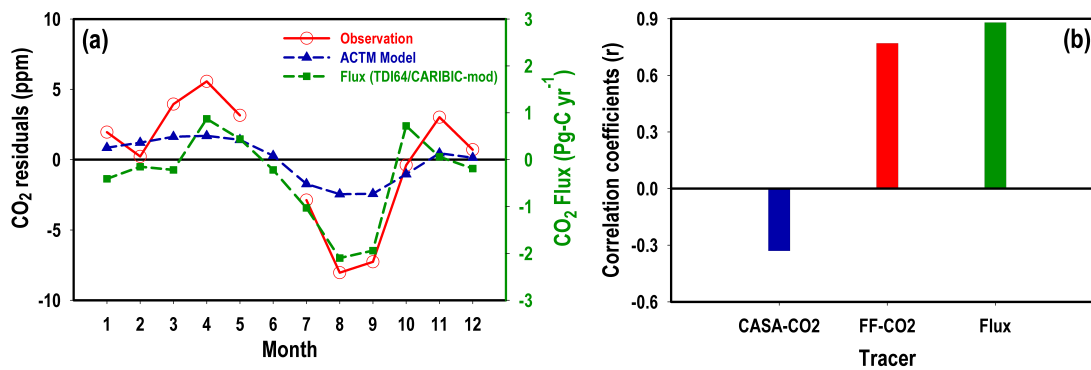


Figure 11: (a) The red circles and blue triangles show the mean seasonal cycles of CO_2 (in ppm) using afternoon values only, calculated from measurements and model over Ahmedabad. The green triangles show the seasonal cycles of CO_2 flux over South Asia, calculated from TDI64/CARIBIC-modified inverse model as given in Patra et al. (2011) (Figure 3d). (b) Blue bar and red bar shows the correlation coefficient (r) of model CO_2 concentration of biospheric tracer and fossil fuel tracer component with observed concentrations of CO_2 taking the entire annual time series of daily mean data, respectively. The green bar shows the correlation coefficient between the monthly residuals of afternoon mean only and the CO_2 flux over South Asia.